Ocean Dynamics (2023) 73:699–727
https://doi.org/10.1007/s10236-023-01577-5

Evaluation of seagrass as a nature-based solution for coastal protection in the German Wadden Sea

Benjamin Jacob[1] · **Tobias Dolch**[2] · **Andreas Wurpts**[3] · **Joanna Staneva**[1]

Received: 19 April 2023 / Accepted: 14 September 2023 / Published online: 18 October 2023

Abstract
Global climate change increases the overall risks for coastal flooding and erosion. Meanwhile, nature-based solutions (NbS) are increasingly becoming a focus of coastal protection measures to improve the climate adaptability. In this study, the present and potential future role of seagrass in coastal risk reduction strategies were explored for the highly energetic Wadden Sea area of the German Bight. The methodology in this study combined seagrass coverage data (*Zostera marina* and *Zostera noltei*) obtained by field surveys and what-if scenario simulations using the SCHISM unstructured grid model framework, coupling hydrodynamics, waves, sediments, and a seagrass module. The results suggest that the introduction of seagrass meadows locally can reduce both current velocities and significant wave heights in the order of up to 30% in the deeper areas and above 90% in the shallow areas. Reduction in bottom shear stress of a similar relative magnitude significantly reduced sediment mobilisation on the order of 2 g/L in the 95th quantile of bottom layer sediment concentrations. Effectively altering hydromorphodynamic conditions favouring sediment accumulation, seagrass expansion could help tidal flats height growths to keep up with SLR, thus further maintaining the bathymetry-induced tidal dampening and lowering flooding and erosion risks as well the amount of energy at dike infrastructure. The accumulated effect of seagrass under calm weather conditions is considered more important than the increased attenuation in absolute values it provides during extreme conditions. The overall conclusion is that seagrass expansion could be a useful addition to engineered coastal protection measures.

Keywords German Bight · Wadden Sea · Seagrass · Unstructured grid modelling · Nature-based solutions · Sensitivity study

1 Introduction

An accelerated rate of sea level rise (SLR) and the trend of increasing occurrences and intensities of extreme sea level (Menéndez and Woodworth 2010) and wave events (Izaguirre et al. 2011) are leading to an increased risk for many coastal landscapes in Europe (Vousdoukas et al. 2017) and globally (Nicholls 2011) in terms of coastal hazards such as erosion, land loss, flooding, and saltwater intrusion (IPCC report summary for policymakers (Allan et al. 2021)). Within estuaries, the risk of compound flooding events, during which drivers from different areas (meteorology, hydrology, and oceanography) constructively combine to cause increased water levels (Couasnon et al. 2020), could increase due to the more frequent and longer extreme discharge events, as expected under global warming projections (Alfieri et al. 2015).

Our study areas are the multiple tidal inlet systems of the North Frisian Wadden Sea (NFWS) and East Frisian Wadden Sea (EFWS), located in the German part (German Bight, Fig. 1) of the southeastern North Sea. Modelling studies addressing the isolated (i.e., without bathymetric adaptations) impact of SLR for the European continental shelf predicted a strong non-linear response of the dominant M2-tidal component in the North Sea leading to an increased M2 tidal amplitude in the southeastern German Bight and the Dutch Wadden Sea (Pickering et al. 2012; Arns et al. 2015), as well as increased extreme water levels for large parts of the North Sea area (Arns et al. 2015). This response was largely attributed to reduced frictional damping and was most pronounced in the shallow Wadden Sea areas, where the tidal

✉ Benjamin Jacob
benjamin.jacob@hereon.de

[1] Institute of Coastal Systems - Analysis and Modeling, Helmholtz-Zentrum Hereon, Geesthacht, Germany

[2] Biosciences, Alfred Wegener Institute, List, Germany

[3] Forschungsstelle Küste, Niedersächsischer Landesbetrieb für Wasserwirtschaft, Küsten- und Naturschutz, Norden, Germany

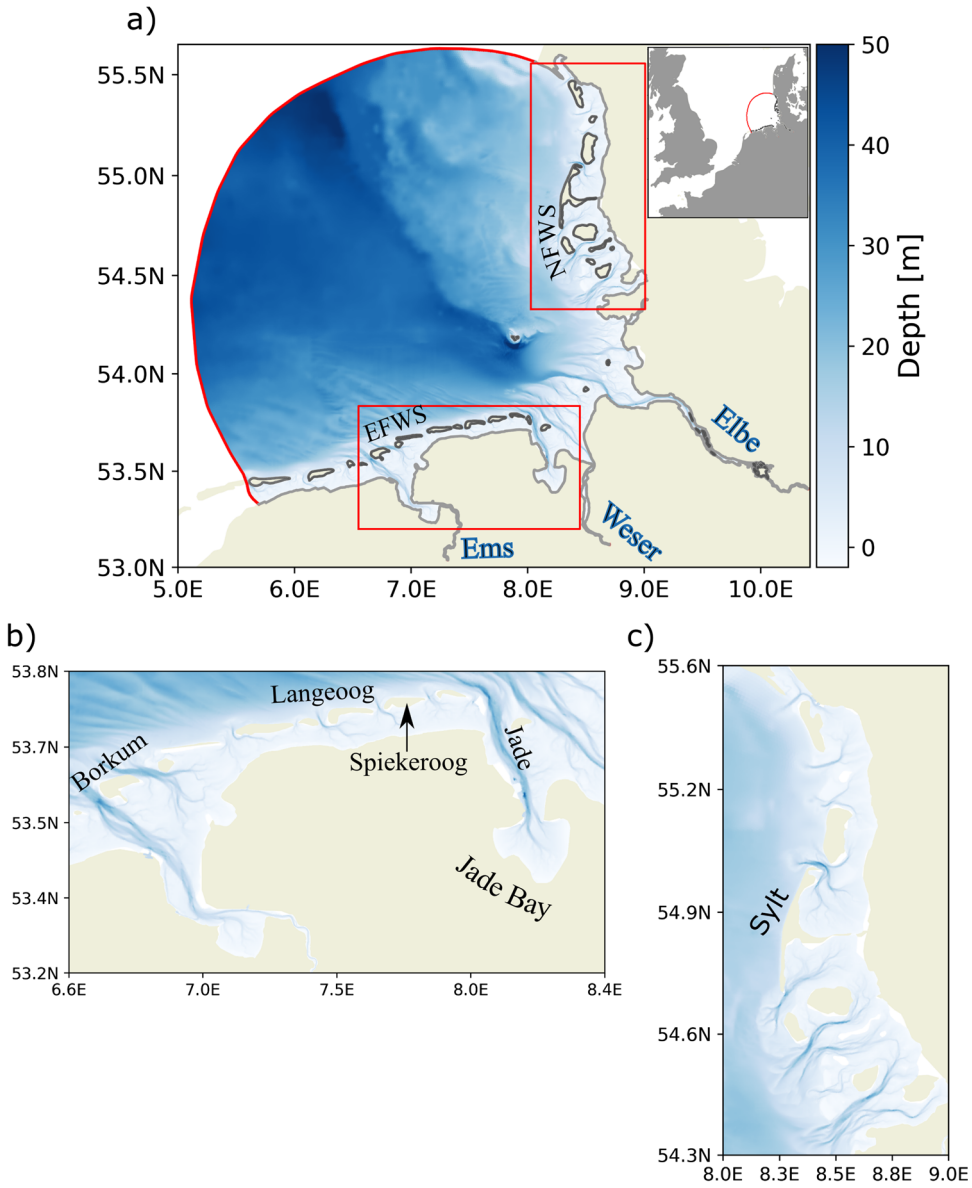

Fig. 1 Overview map of the German Bight model domain (**a**, open ocean boundaries are depicted as red lines, land boundaries as grey ones) and seagrass recovery experiment focus areas, East Frisian Wadden Sea (EFWS, **b**), and North Frisian Wadden Sea (NFWS, **c**)

wave is subject to pronounced nonlinear transformation and becomes asymmetric between flood and ebb. As indicated by the SLR experiments in Stanev et al. (2006), a sea level increase of 1 m, could lead to a reversal of the tidal current asymmetry (from ebb to flood dominant) in the tidal inlet systems of the EFWS.

To date, the recent morphological characteristics of the Wadden Sea (NFWS and EFWS) analysed by Benninghoff and Winter (2019) indicate an accumulation of sediments, which for most tidal flat areas exceeds the rates of SLR. However, this accumulation occurs with an increase in subtidal mean depth that results in a steeper channel flat transition. Benninghoff and Winter (2019) found that the sediment import is about twice the amount needed to scale linearly with SLR, but argued that the height growth of the intertidal area above SLR will result in a negative feedback towards accumulation via a reduced inundation time and accommodation space. With expectations of changing hydrological cycles, feeding of ebb-tidal deltas, altered hydrodynamics, and not fully identified sediment pathways, the ability to maintain pace with SLR remains unclear on the supply side.

While the NFWS inlet system has not been studied to the same extent as the EFWS system, due to the similarity in tidal range and presence of similar morphological features (tidal basins protected by island chains), the dynamics are subject to the same fundamental controls and experience similar morphological changes.

Taking into account the changed water levels and potential future bathymetric changes, Wachler et al. (2020) demonstrated that for 0.8 m of SLR, deepened tidal channels and

0.5 m of tidal flat height growth in the German Wadden Seas (i.e., not completely maintaining pace with SLR) can mostly compensate the effects (e.g., changed tidal asymmetry) of SLR.

This outcome emphasises the importance of accounting for potential bathymetric changes in regional projections. Within the last three decades, morphological changes observed in the coastal German Bight (Benninghoff and Winter 2019) have been shown (Jacob and Stanev 2021) to play a larger role than SLR in shaping the tidal characteristics of the EFWS over the corresponding temporal horizon.

Effective coastal protection measures have become increasingly important in the context of global SLR; however, coastal flooding and erosion represent severe risks even under current (storm) conditions. To counteract these risks, historic and past coastal protection strategies have mainly involved 'hard' ('grey') engineering solutions, such as the construction of dikes, groynes, breakwaters, sea walls, and other types of physical barriers (French 2002). However, these measures are expensive, prevent fluxes between land and sea, often represent extensive interference with the natural systems, and occasionally have unwanted side effects, including enhancing coastal erosion and negatively impacting the environment (Temmerman et al. 2013).

Therefore, in recent decades, there has been a paradigm shift towards increasingly applying nature-based solutions (NbS) for coastal protection (Temmerman et al. 2023; Morris et al. 2018). Rarely, under certain conditions, NbS could replace technical infrastructure, for example, NbS could be used to reduce wave heights (30–70%) as vegetation could be comparable to low-crested breakwaters if wave heights remain moderate and there is room in an area for widespread vegetation (Narayan et al. 2016). Typically, however, a NbS is most suitable as supplementary approach accompanying the hard constructive measures (van Wesenbeeck et al. 2016), e.g., foreshore ecosystems like tidal marshes can help decrease hydrodynamic loads at the dyke).

NbS ('green' solutions) commonly use natural elements as 'building bricks' to construct a protective system. These solutions include coastal vegetation (e.g., seagrass beds and salt marshes in temperate regions and mangroves in subtropical and tropical regions) to attenuate energy and facilitate sediment accumulation, sand nourishment to counteract land loss and increase frictional damping, mussel beds to serve as additional roughness element, or extensive flood plains to provide an area for energy to be distributed. These measures can help to attenuate natural forces to reduce the erosive potential or to utilise them for the maintenance or accumulation of coastal wetlands. In comparison to engineered solutions, NbS are inexpensive and less intrusive and allow for dynamic coastal development (Bergillos et al. 2018). Therefore, these solutions are more adapted to climate change effects and consistent with the goal to keep the coasts in an overall natural state and to counteract the ongoing deterioration of coastal systems (Krämer 2018).

For different ecosystems in a meta-analysis, Ferrario et al. (2014) determined the wave height reductions caused by coral reefs (70%), mangroves (31%), salt marshes (72%), and seagrass/kelp beds (36%).

Here, we focus on the role of seagrass as a NbS, which constitutes the coastal vegetation occurring in the intertidal areas of the German Wadden Sea. In the last decade, there has been a growing number of activities aimed at the recovery (Dolch et al. 2013) and restoration (Boudouresque et al. 2021; Govers et al. 2022) of seagrass, alongside various studies (Temmerman et al. 2013) that acknowledge the benefits of implementing NbS in many regions of the world. Vegetated tidal wetlands provide a range of ecosystem services and benefits, including the following:

- The surface area of plant shoots and leaves interacts with the flow as a dissipative element, favouring wave breaking, increasing the surface roughness, and effectively attenuating the energy of short waves (Paul et al. 2012; Temmerman et al. 2023) and currents (Fonseca et al. 1982). However, the presence of tidal currents negatively influences the overall wave attenuation capacity of seagrass (Paul et al. 2012). In mangrove tidal wetlands, however, there is some evidence that these wetlands can reduce storm surge water levels to a small extent (Montgomery et al. 2019); for seagrass, this effect is negligible, and the increase in sea level by several meters renders its potential to attenuate waves much less effective.
- The root and rhizome network of seagrass has a stabilising effect on the seabed and increases resistance to erosion and resuspension, and synergistically, the dissipative effect of the submerged plant body enhances sediment deposition (sediment trapping) and promotes tidal wetland height growth, especially in sheltered areas, where seagrass has higher chances of persisting (Koch et al. 2001; de Boer 2007. Changes in hydrodynamic/sedimentary conditions can promote further growth of seagrass population in a positive feedback loop.
- Beyond the physical protection seagrass offers, expanding seagrass beds can also play a supporting role in slowing global warming by acting as a carbon sink (blue carbon, Duarte et al. (2013)).
- Seagrass is ecologically highly valuable with a range of ecological co-benefits, because seagrass meadows serve as a habitat, food source, and nursery ground (Costanza et al. 1997).

Generally, seagrass can only grow under fairly calm hydrodynamic conditions and in water of sufficient quality (Temmerman et al. 2023). In addition, seagrass is sensitive to many environmental conditions, such as strong kinetic

energy (e.g., storms can inflict heavy damage), pollution, and the direct and indirect effects of eutrophication, low-light conditions, and high temperatures (Chefaoui et al. 2018); thus, global warming is considered a severe threat to seagrass populations worldwide.

As seagrass is sensitive to a variety of parameters and responds quickly to changing environmental conditions, it is used as an indicator species for ecosystem health in the Marine Strategy Framework Directive (MSFD) and the EU Water Framework Directive (WFD).

To increase the success rate of seagrass (re)introduction, the transplantation of large amounts of seagrass to create new patches appears to be a successful strategy that reduces hydrodynamic stress and increases the plant survival rate (Irving et al. 2014; Gagnon et al. 2021). Another approach is to improve the environmental conditions for seagrass in order to enable its natural recovery and expansion. In cases where NbS alone cannot provide the required protection, Bouma et al. (2014) advocate the combination of engineering solutions and NbS. Furthermore, the use of combined approaches involving different NbS (e.g., combining sand nourishments with vegetation) can have also synergistic effects (Chen et al. 2022).

The previously mentioned effects of seagrass on hydrodynamics, which are considered in the undertaken model studies, are also schematised in Fig. 2, comparing the situations without (a), with submerged seagrass (b), and with emergent seagrass (c).

Several modelling studies, accounting for the effect of vegetation on hydrodynamics, have been conducted in recent decades (Temmerman et al. 2005; Horstman et al. 2014; Temmerman et al. 2013; Beudin et al. 2017). Many of these modelling approaches involved structured or curvilinear grids. However, as noted by Zhang et al. (2020), these approaches are limited in their applicability to field-scale applications due to the use of explicit time stepping and the resulting restrictions for resolution. Enhancing an unstructured grid model for first-order vegetation effects, Zhang et al. (2020) demonstrated a sufficient correlation between laboratory experiments and numerical experiments, reasonably replicating this scale and demonstrating the role of vegetation in the San Francisco Bay-Delta. Using the unstructured grid XBeach morphodynamic model, Chen et al. (2022) analysed the combined effects of sand nourishment and a seagrass plantation as hybrid NbS. The results showed synergistic effects in terms of mitigating sediment transport in a sheltered nearshore area. In a study on seagrass as NbS against storm surges in the Northern Adriatic Sea, Pillai et al. (2022) found that the spatial arrangement pattern of seagrass is particularly important for the attenuation of waves and currents.

In this study, we address the sensitivity of coupled hydro-, wave-, and sediment dynamics in different simplified seagrass recovery scenarios for the German Bight and contrast them with the coastal protection offered by the present-day seagrass cover derived from coastal vegetation data (Dolch et al. 2017, personal communication and unpublished data).

In particular, we address the following questions: (I) by what amount can the strengths of currents and waves be reduced due to the presence of seagrass, and how are coastal dynamics impacted in general? (II) How does attenuation in a densely populated meadow compare to that in a more sparsely populated meadow, and how do recovery scenarios compare that focus different zones of the intertidal? (III) Are these results comparable for the EFWS and NFWS? And finally,

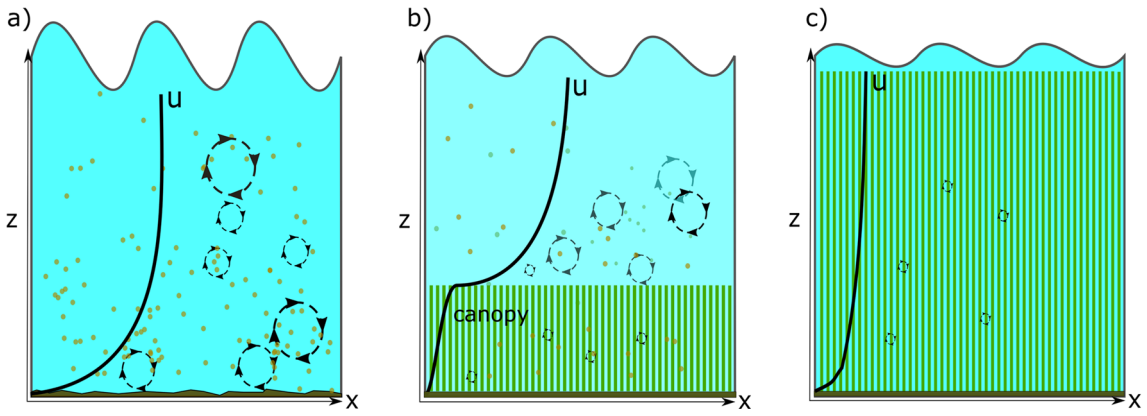

Fig. 2 Schematic of the effect of seagrass on hydrodynamics, waves, and sediment dynamics. **a** shows the boundary layer flow without seagrass and high shear generation in the rough bottom layer. **b** is the situation with submerged canopy (green lines), which dampens velocities in the bottom layer and increases shear generation above the canopy. **c** is the situation with fully emerged canopy, which dampens velocities over the whole water column and reduces shear over the whole water column. The schematic velocity profile u(z) is represented by the black line, and the black circles with arrows are symbolic of the amount of turbulence. The reduced erosive sediment mobilisation due to reduced bottom reaching shear is indicated by the reduced number of SPM (brown dots) and the wave attenuation as reduced wave height shown at the top of the water column. The figure is adapted from Fig. 4 in Leonardi et al. (2018)

(IV) do the accumulative effects during calm weather periods outweigh the importance of attenuation provided during extreme events, considering the risks of coastal flooding and erosion?

The experiments were conducted using the Semi-implicit Cross-scale Hydroscience Integrated System Model (SCHISM) modelling system (Zhang et al. 2016), which operating on unstructured grids allows covering the tidal wetlands in high-resolution. The consideration of vegetation-induced turbulence and friction within the vegetation module of SCHISM enables the framework to simulate the first-order vegetation impact on hydrodynamics, representing vegetation as rigid cylinders (Zhang et al. 2020).

The German Bight SCHISM configuration is based on Stanev et al. (2019), as this configuration reproduces coastal hydrodynamics and overall sediment dynamics well and has proven to be a useful tool for studying the sensitivities of the coastal systems, such as their responses to changing morphologies (Jacob and Stanev 2021). The integrated wave module WWMIII (Roland et al. 2012) allows us to study coupled effects, which play an important role in the North Sea domain (Schloen et al. 2017; Staneva et al. 2014).

In the following sections of this paper, first, the seagrass data, the numerical model with its different compartments, and the design of the numerical seagrass recovery experiments are described (Sect. 2). Then, an analysis of the sensitivity of hydro-, wave-, and sediment dynamics with respect to the seagrass distribution is presented in Sect. 3 and is further discussed in Sect. 4, until we close the paper with the conclusions and outlook in Sect. 5.

2 Data and methods

2.1 Seagrass data

The seagrass population in the area of the Wadden Sea consists of the species *Zostera marina* (*Z. marina*) and *Zostera noltei* (*Z. noltei*), of which the physiologically smaller species *Z. noltei* is by far more dominant.

The seagrass data for the East Frisian Wadden Sea (EFWS) were kindly provided by the NLWKN and can be accessed via the Geodata Portal of the federal state Lower Saxony (https://mdi.niedersachsen.de/HeronKaDI/JAVA_SCRIPT/37_Portal/, last visited April 19, 2023). The data for the more densely populated North Frisian Wadden Sea (NFWS) (compared to the very sparse seagrass population in the EFWS) were provided by Tobias Dolch, who conducts the official seagrass monitoring in Schleswig-Holstein on behalf of the Landesamt für Landwirtschaft, Umwelt und ländliche Räume Schleswig-Holstein (LLUR) and the Landesbetrieb für Küstenschutz, Nationalpark und Meeresschutz Schleswig-Holstein - Nationalparkverwaltung (LKN). Seagrass in the NFWS has shown a strong recovery since the late 1990s (Dolch et al. 2013). In both cases, the data describe, among other parameters, the—for us most important—relative areal coverage of seagrass within a seagrass meadow, as well as the shoot density within a bulge within the meadow, which is multiplied to the total coverage. The data on seagrass meadows and their coverages are gathered in the field by foot, circling a seagrass meadow and recording its boundaries via GPS/GNSS in order to determine the shape, position, and areal extent. In a second step, transects crossing through the seagrass meadow are set in order to estimate the cover density and species composition of the inner part of the meadow. Later these data are extrapolated to the entire area of the seagrass meadow. The GPS data are processed using GIS and are provided as GIS shapefiles, containing the before-mentioned parameters stored as polygons. Based on the field surveys and supported by aerial photographs as well as by pictures taken in the field, the cover density of the seagrass meadow is subsequently further edited: the spatial distribution of the cover density was divided into 20% intervals.

Since the formulation of vegetation effects on the model is based on density, the areal coverage assessed in field surveys was converted to shoot densities. The assessment of seagrass coverage is supported and accompanied by the counting of representative shoot densities in the field using a measuring frame. To generalize the shoot densities, the shoot numbers counted by applying the frame within several seagrass beds were averaged for each areal coverage class. The extrapolated conversion relations are given in Table 1.

2.2 Numerical model

2.2.1 Hydrodynamic model

To conduct the numerical seagrass recovery scenarios, the semi-implicit cross-scale hydroscience integrated system model (Zhang et al. 2016) is used as hydrodynamic core and

Table 1 Interval of seagrass areal coverage in data and corresponding shoot density (N_v) provided to the model

Areal coverage (%)	Shoots (1/m^2)
5–19.9	450
20–39.9	1130
40–59.9	1530
60–79.9	3540
80–100	7360

run in coupled mode with the 3rd-generation wave model WWMIII (Roland et al. 2012), which is implemented as part of the SCHISM framework. The seagrass influence on hydrodynamics is parameterised in SCHISM as an additional friction term in the momentum equation.

SCHISM itself is a derivative product of the Semi-implicit Eulerian-Lagrangian Finite Element model (SELFE, Zhang and Baptista 2008). It solves the Reynolds-averaged Navier–Stokes equations under hydrostatic and Boussinesq approximations on unstructured (potentially mixed quadrangular-) triangular grids. Time step iteration is done with a semi-implicit scheme, ensuring numerical stability and efficiency of the model.

For a precise momentum advection, it uses a higher-order Eulerian-Lagrangian method (ELM). Tracer transport equations are solved with a 2nd-order total variation diminishing (TVD) scheme. The turbulence closure model uses the generic length scale (GLS) formulation by Umlauf and Burchard (2003) in k-ϵ parameterisation. SCHISM simulates the process of wetting and drying, where in our case a minimum water column depth of 5 cm is used as threshold for an area to be considered dry.

We use SCHISM with a grid configuration for the German Bight, that, with some slight grid modifications, is based on the model presented by Stanev et al. (2019) and currently is operated at Hereon on pre-operational mode. The model area consists of 476 k nodes and 932 k triangular and quadrangular elements, with the horizontal resolution, varying between a maximum of 1.5 km at the open boundary and a minimum of 50 m in the estuaries. The vertical dimension is resolved using 21 terrain-following sigma coordinates. Within the EFWS and NFWS constituting our study area, the resolution ranges between 100 and 300 m.

Model initialisation and ocean boundary forcing are derived from the CMEMS AMM15 operational product, the latter being provided as hourly time series for the variables, temperature, salinity, sea surface elevation, and 3D velocities. Furthermore, temperature and salinity fields are relaxed towards the CMEMS forcing in a 20-km zone from the open ocean boundary. The atmospheric forcing is derived from hourly output fields of the EU domain icon model of the German Weather Service (DWD) and encompasses the atmospheric pressure at sea level, surface temperature, and specific humidity (evaluated at the standard height of 2 m) and the surface wind speed (evaluated at the standard height of 10 m), as well as the solar radiation. River discharge is applied based on climatological data for the rivers Ems, Weser, Elbe, and Eider.

The formulation of the seagrass interaction is in detail described in Zhang et al. (2020), following the notation of which the frictional effect of seagrass is introduced as additional form drag term as last term in the momentum equation (following the terms contained in $\boldsymbol{f}$, the barotropic pressure gradient, and the vertical eddy viscosity term):

$$\frac{D\boldsymbol{u}}{dt} = \boldsymbol{f} - g\nabla\eta + \boldsymbol{m_z} - \alpha|\boldsymbol{u}|\boldsymbol{u}L(x,y,z) \tag{1}$$

$\boldsymbol{f}$ encompasses the numerically explicitly treated terms

$$\boldsymbol{f} = f(v,-u) - \frac{g}{\rho_0}\int_z^\eta \nabla\rho d\zeta - \frac{\nabla p_A}{\rho_0} + \boldsymbol{F_m} + \boldsymbol{R},$$

which include Coriolis, baroclinic and atmospheric pressure gradient, horizontal viscosity ($\boldsymbol{F_m}$), and additional forces, such as in our case the radiation stress ($\boldsymbol{R}$) from the couple wave model WWM. The vegetation drag term of (1)

$$\alpha(x,y) = D_v N_v C_{Dv}/2$$

([α] =m^{-1}) parameterises the vegetation density-related frictional scaling as the product of the individual's stem diameter (D_v), the vegetation density (N_v, given as number of stems per m^2), and CD_v, the bulk form drag coefficient, typically ranging between values of 0 and 3 (Nepf and Vivoni 2000; Tanino and Nepf 2008) and, in our case, chosen as 1. The vegetation terms as for the 3D and 2D cases (here, we do not use a vertical polymorphism and the 3D case is valid over the entire model domain) are

$$L(x,y,z) = \begin{cases} \mathcal{H}(z_v - z), 3D \\ 1, 2D \end{cases}$$

$$\mathcal{H}(x) = \begin{cases} 1, x \geq 0 \\ 0, x < 0 \end{cases}$$

with $\mathcal{H}$ being the Heaviside step function and z_v the z-coordinate of the canopy height. The turbulence induced by vegetation is represented in the model as additional source for turbulent kinetic energy ($\boldsymbol{k}$):

$$\frac{D\boldsymbol{k}}{Dt} = \frac{\partial}{\partial z}(\nu_{\boldsymbol{k}}^{\psi}\frac{\partial \boldsymbol{k}}{\partial z}) + \nu\boldsymbol{M}^2 + \kappa N^2 - \epsilon + c_{fk}\alpha|\boldsymbol{u}|^3\mathcal{H}(z_v - z) \tag{2}$$

and mixing length (ψ)

$$\frac{D\psi}{Dt} = \frac{\partial}{\partial z}(\nu_\psi\frac{\partial\psi}{\partial z}) + \frac{\psi}{\boldsymbol{k}}[c_{\psi 1}\nu\boldsymbol{M}^2 + c_{\psi 3}\kappa N^2 - c_{\psi 2}\epsilon F_{wall} + c_{f\psi}\alpha|\boldsymbol{u}|^3\mathcal{H}(z_v - z)] \tag{3}$$

2.2.2 Wave model

The coupled wave model WWMIII (Roland et al. 2012) is a 3rd-generation spectral wave model that solves the wave

action balance action equation on an unstructured triangular mesh, which in coupled mode is identical to the SCHISM grid, as also is the sub-domains MPI-parallelisation. The wave action equation

$$\frac{\partial}{\partial t}N = \nabla_{\boldsymbol{X}}(\dot{\boldsymbol{X}}N) + \frac{\partial}{\partial \sigma}(\dot{\Theta}N) + \frac{\partial}{\partial \Theta}(\dot{\sigma}N) = S_{tot} \tag{4}$$

describes the dynamic of the wave action,

$$N(t, \boldsymbol{X}, \sigma, \theta) = \frac{E_{(t,\boldsymbol{X},q,\theta)}}{\sigma} \tag{5}$$

where E is the variance density of sea level elevations, σ is the relative wave frequency, and θ is the wave direction. In the different phase spaces, the advection velocities are given by

$$\dot{\boldsymbol{X}} = \boldsymbol{c}_{\boldsymbol{X}} = \frac{d\boldsymbol{X}}{dt} = \frac{d\omega}{d\boldsymbol{k}} = c_g + \boldsymbol{U}_{A(\boldsymbol{k})} \tag{6}$$

$$\dot{\Theta} = c_0 = \frac{1}{\boldsymbol{k}} = \frac{\partial \sigma}{\partial d}\frac{\partial d}{\partial m} + \boldsymbol{k} \cdot \frac{\partial \boldsymbol{U}_{A(\boldsymbol{k})}}{\partial s} \tag{7}$$

$$\dot{\sigma} = c_\sigma = \frac{\partial \sigma}{\partial d}\left(\frac{\partial d}{\partial t} + \boldsymbol{U}_{\boldsymbol{A}} \cdot \nabla_x d\right) - c_g \boldsymbol{k}\frac{\partial \boldsymbol{U}_{A(\boldsymbol{k})}}{\partial s} \tag{8}$$

in which s and m denote the coordinates along and perpendicular to the direction of wave propagation, respectively. $\mathbf{X}$ represents 2D space in Cartesian geographical coordinates (x, y), d is the water depth, $\mathbf{k}$ is the wave number vector (with $k = |\boldsymbol{k}|$), c_g is the group velocity, ω is the absolute wave frequency, and $\nabla_{\mathbf{X}}$ is the gradient operator in the geographical space. The group velocity (c_g) is calculated from the linear dispersion relation.

The source function S_{tot} includes the wind energy input S_{in}, the nonlinear interactions in deep water (S_{nl4}) and shallow water (S_{nl3}), and the energy dissipation in deep and shallow water due to white capping (S_{ds}) and wave breaking (S_{br}). Furthermore, it encompasses the dissipation due to bottom friction (S_{bf}) and vegetation $(S_{d,veg})$. We use WWM configured with ST4 physics, and the receptive formulations of the terms apart from the vegetation can be found in detail (Roland et al. 2012).

$$\frac{DN}{Dt} = S_{total} = S_{in} + S_{nl4} + S_{ds} + S_{nl3} + S_{br} + S_{bf} + S_{d,veg} \tag{9}$$

The wave breaking in shallow water is formulated after Battjes and Janssen (1978). The formulation of wave dissipation by bottom friction is based on JONSWAP (Joint North Sea Wave Atmosphere Program, Hasselmann et al. 1973).

The Wave-vegetation sink term $S_{d,veg}$ in WWM follows Suzuki et al. (2012) and is implemented in WWM similarly to the description provided by Abdolali et al. (2022) for Wave Watch 3 (WW3):

$$S_{d,veg} = -\sqrt{\frac{2}{\pi}}g^2 C_d b_v N\left(\frac{\bar{k}}{\bar{\sigma}}\right) * \frac{3\sinh^3(\bar{k}ah) + 3\sinh(\bar{k}ah)}{3\bar{k}\cosh^3(\bar{k}h)}\sqrt{E_{tot}}E(\sigma, \Theta) \tag{10}$$

In that, E_{tot} is the integral of wave energy $E = \frac{1}{8}\rho g H^2$:

$$E_{tot} = \int_0^{2\pi}\int_0^{\infty} E(\sigma, \Theta)d\sigma\Theta)^{-1} \tag{11}$$

$\bar{\sigma}$ and $\bar{k}$ are the mean frequency:

$$\bar{\sigma} = \left(\frac{1}{E_{tot}}\int_0^{2\pi}\int_0^{\infty}\frac{1}{\sigma}E(\sigma, \Theta)d\sigma\Theta\right)^{-1} \tag{12}$$

and mean wave number

$$\bar{k} = \left(\frac{1}{E_{tot}}\int_0^{2\pi}\int_0^{\infty}\frac{1}{\sqrt{k}}E(\sigma, \Theta)d\sigma\Theta\right)^{-1} \tag{13}$$

WWM is operated at a timestep of 240 s, exchanging information every third iteration of the hydrodynamical model, which is operated at a time step of 80 s. Spectral wave boundary data to force the WWM configuration in the German Bight was generated running a Wave Watch 3 configuration covering the north eastern Atlantic and the North Sea domain. This configuration was forced using wind velocities from the DWD icon model output.

2.2.3 Sediment model

For the simulation of sediment dynamics, we couple SCHISM with the 3D sediment model SED3D contained in the SCHISM modelling framework. The sediment model was adapted from the community Sediment Transport Model (Warner et al. 2008) and ported as an unstructured grid implementation within the SCHISM modelling framework Pinto et al. 2012. The sediment model resolves the processes of erosion, deposition, bed load transport, and suspended load transport for non-cohesive sediments. The transport of suspended sediment concentration (C) is computed by the advection–diffusion equation enhanced by the term for vertical settling for each sediment class (q):

$$\frac{\partial C_q}{\partial t} + u\frac{\partial C_q}{\partial x} + v\frac{\partial C_q}{\partial y} + w\frac{\partial C_q}{\partial z} = \frac{\partial}{\partial z}\left(\kappa\frac{\partial C_q}{\partial z}\right) + ws, q\frac{\partial C_q}{\partial z} + F_h \tag{14}$$

Further in the equation, u, v, and w denote the 3D velocity components, κ is the eddy diffusivity, $w_{s,q}$ is the settling

velocity for sediment class q, and F_h is the horizontal diffusion. The sediment settling velocity is computed for each class following Soulsby (1997) as

$$ws, q = \frac{\nu_a}{d_{50,q}}[(10.36^2 + 1.049D_{*,q}^3)^{0.5} - 10.36] \quad (15)$$

with ν_a being the kinematic viscosity of water, $d_{50,q}$ the median grain size diameter of sediment class q, and $D_{*,q}^3$ the dimensionless sediment diameter, which is computed as follows:

$$D_{*,q}^3 = [\frac{g(s-1)}{\nu_a^2}]^{\frac{1}{3}} d_{50,q} \quad (16)$$

In that g is the gravitational acceleration, $s = \rho_{s,q}/\rho_w$ is the specific density, and qs, q, and qw are the reference densities of sediments and water, respectively.

The sediment exchange between the bed and the water column is implemented via sink and source terms that act on the bottom computational cell.

The depositional flux is calculated as the product of the settling velocity and the concentration at the bottom computational cell (C_1):

$$D_q = w_{s,q} C_1 \quad (17)$$

The erosion flux, E_q, is given following the formulation of Ariathurai and Arulanandan (1978):

$$E_q = E_{0,q}(1-p) f_q (\frac{\tau_{s,f)}}{\tau_{cr,q}} - 1) \text{ if} \tau_{s,f} > \tau_{cr,q} \quad (18)$$

$$\tau_{cr,q} = \theta_{cr,q} g d_{50,q} (\rho_s - \rho_w) \quad (19)$$

In that, $E_{0,q}$ is an empirical bed erodibility constant (ranging between 10^{-4} to 10^{-2} $m^{-2}s^{-1}$), p is the sediment porosity in the upper soil layer, f_q is the volumetric fraction of sediment class q, $\tau_{cr,q}$ is the sediment class specific critical shear stress, and $\tau_{s,f}$ is the absolute value of bed shear stress. $\theta_{cr,q}$ is the dimensional critical shear stress, which is derived from the critical Shields parameter, and is computed after Soulsby et al. (1997) as

$$\theta_{cr,q} = \frac{0.3}{1 + 1.2D_{*,q}} + 0.055[1 - e^{(-0.022)D_{*,q}}] \quad (20)$$

The bottom shear stress is computed as

$$(\tau_{bx}, \tau_{by}) = (\gamma_1 + \gamma_2\sqrt{u^2 + v^2})(u, v) \quad (21)$$

which follows either a linear, quadratic, or logarithmic bottom friction, via different choices of the linear (γ_1) and quadratic (γ_2) drag coefficients

$$(\tau_{bx}, \tau_{by}) = (\gamma_1 + \gamma_2\sqrt{u^2 + v^2})(u, v) \quad (22)$$

Using the logarithmic formulation, the vertical logarithmic profile in the bottom boundary layer follows

$$|u| = \frac{u_*}{\kappa_0} \ln(\frac{\delta_b}{z_0}) \quad (23)$$

where $|u|$ is the velocity magnitude, $u_* = \sqrt{(|\tau_{bx}| + |\tau_{by}|)/\rho}$ is the friction velocity, $\kappa = 0.4$ is the von Kármán constant, z_0 is the bottom roughness length, and δ_b is the thickness (m) of the bottom computational layer.

The impact of sediment concentration on the water density is considered via an extension in the equation of state:

$$\rho = \rho_w + \sum_{q=1}^{Nsed} \frac{C_q}{\rho_{s,q} - \rho_w}, \quad (24)$$

in which ρ is the local fluid density considering the combined effect of temperature, salinity, and sediments, ρ_w is the water density determined by solely temperature and salinity, and Nsed is the number of sediment classes used.

We have configured it (analogous to Stanev et al. 2019) for eight sediment classes with median grain sizes (d50) of 0.06 mm, 0.07 mm, 0.1 mm, 0.125 mm, 0.24 mm, 0.5 mm, 1.0 mm, and 2.0 mm. They are erodible from an infinite bottom pool of sediments, for which the abundance of the different grain sizes is given as bed fractions derived from maps described by Milbradt et al. (2015), based on surveys conducted by the Bundesanstalt für Wasserbau in the German Bight (Valerius et al. 2015). At the open boundaries, a zero sediment gradient is employed. The model was operated morphostatically.

2.2.4 Validation

A general validation of the German Bight model was presented by Stanev et al. (2019). For the present study, a comparison with different tide gauge stations and simulations for September and October using the Ref scenario for different stations along the German Bight is given in the supplementary material (Fig. S1). The overall correlation between the model and observations ranges from 0.95 to 0.99%. The root mean squared error is mostly between 0.2 and 0.3 m. The relative standard deviation fluctuates around the 0.9 mark. Overall, the model reproduced the tidal amplitudes and timing well. The storm surge peaks from Herwart were also timed correctly but slightly underestimated in the EFWS (approximately 20–30 cm). At Cuxhaven, where the highest tides occur among the German Bight stations, the peak water levels of about 3.6 m measured on the south coast were underestimated by about 20% by the model, which simulated a peak of about 2.9 m. This underestimation is attributed to a lack of energy in the wind forcing, leading

to an underestimation of the wind-driven rise in water level at the southern coast (EFWS) in the hydrodynamic model.

Regarding waves, the validation of the significant wave height at the Fino3 (FN3) and Westerland (WES, near Sylt) buoys, covering the week before and during the storm (supplementary material, Fig. S2), demonstrates that the modelled significant wave height is generally consistent with observations in terms of timing and general trends for HS. However, there is a tendency to underestimate the maximum significant wave height prior to the October 29 storm event at station Fino3. The maximum significant wave heights during Herwart are measured (simulated) to be about 6.9 (6.2) m at Fino3 and about 5.2 (4.8) m at Westerland. The correlation between the model and observations is about 0.959 at FN3 and 0.963 at WES. The root mean squared error amounts to 0.322 m and 0.252 m, respectively. The bias at these stations is about 0.115 and −0.06 m, respectively.

2.3 Scenarios

Different scenario runs (see Table 2 and Fig. 3 for an overview) were conducted running SCHISM coupled with both sediments and waves. The influences of the current seagrass population size scenario (E1; Ref), hypothetical extended expansion scenarios (E3-E5), and the complete absence of seagrass scenario (E2) were explored with a set of five experiments.

The experiments were constructed as academic 'what-if scenarios' evaluating the hypothetical dampening effect of seagrass at different extents and in different regions of the Wadden Sea. In contrast to other studies that attempt to anticipate the potential emergence of seagrass or the overall habitat suitability (e.g., Bittner et al. 2020), we did not evaluate the effect of hydrodynamics on seagrass, only the uni-directional impact of seagrass on hydrodynamics. Hence, the spatial arrangements of seagrass in the scenarios were not constructed assuming the most likely areas for seagrass recovery or recovery volumes. Instead, the scenarios explore the uppermost ceiling of seagrass expansion, as well as the distinguished effect of having seagrass in highly energetic zones where it would interact with stronger currents and wave energy, and analogously the effect of seagrass recovery taking place in the low energetic zone.

Table 2 Interval of seagrass areal coverage in data, and corresponding shoot density (N_v) provided to the model

No.	Name	Seagrass cover
1	Ref	Present-day (data) coverage
2	Blank	None
3	Veg_{max}	Entire WS between −1 and 4 m
4	Veg_{LE}	Shallowest 10% of Veg-Max
5	Veg_{HE}	Deepest 10% of Veg-Max

The (simplified) expansion scenarios encompass the entire area falling into the depth range potentially habitable for seagrass (E3) considering the depth interval from −1 to 4 m in the Wadden Sea (corresponding to Fig. 3 Veg_{max}), which generally corresponds to the vegetated depth range observed in the data. E4 (Veg_{LE} Fig. 3) is the low energy scenario, establishing seagrass beyond the present-day coverage (E1/Ref Fig. 3) on the shallowest 10% (using higher depth as proxy for the more energetic regions further offshore, i.e., the shallow littoral) of the area covered in (E4). Similarly, E5 (Veg_{HE} in Fig. 3) is the high-energy scenario, assuming seagrass recovery in addition to the present-day coverage (E1) on the deepest 10% (i.e., along the channel edges) of the area covered in E3. The shallower subtidal regions are where seagrass is more likely to recover (E4), while in the deeper/more energetic zones (E5), seagrass is likely to be less resilient due to the exposure to larger waves and higher current velocities.

The vegetation effects for the experiments were prescribed via the parameters of α Eq. 1, which is a combination of the following:

- CD_v=1, the plant geometry/property-related drag coefficient, which was chosen as 1 for simplicity purposes (due to lack of existing calibrations).
- D_v, the individual's stem diameter (given at each grid node, there is no explicit species distinction in the model). For E1 (where data on species dominance were gathered), the stem/leaf (i.e., rigid cylinder representation) diameter is based on field observations and is generalised to
  - $D_v = 1.99$ mm for *Z. marina* dominated regions,
  - $D_v = 0.8$ mm for *Z. noltei* dominated regions,
  - and in places of mixed occurrences (i.e., the majority of E1 and all areas in E3-E5) of both species $D_v = 0.8$ was set to the average value.
- The canopy height H_z, which influences the part of the water column that is influenced by seagrass interaction, was set to
  - $H_z = 19$ cm for *Z. marina* dominated regions,
  - $H_z = 9.8$ cm for *Z. noltei* dominated regions,
  - and in places of mixed occurrences (i.e., the majority of E1 and all areas in E3-E5) of both species $H_z = 14.4$ cm was set to the average value.
- Finally, N_v represents the areal coverage given as the number of shoots(cylinders) per m^2, which was derived for E1 from the areal coverage estimates.

For E1, there is spatial variance in the physiological parameters depending on the local species abundance

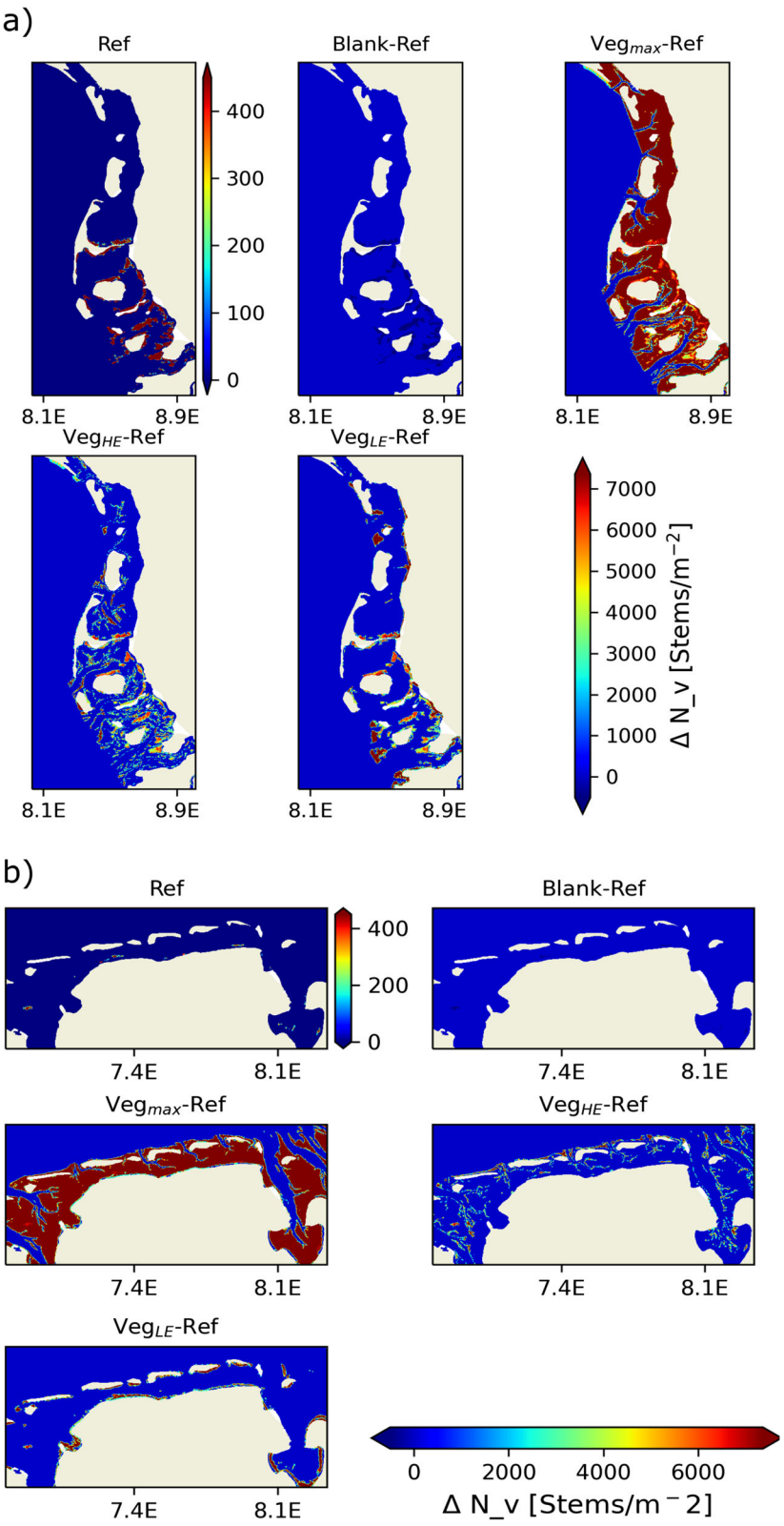

Fig. 3 Seagrass coverage and shoot density in the different seagrass scenarios **a** in the NFWS and **b** in the EFWS. In **a/b** top left: shoot density in reference run, followed by differences of E2-E5 (Table 2) minus reference run

extrapolated from the measurements. For all expansion experiments, for simplicity purposes, we assume a 1:1 ratio of both seagrass species by using the average values for the physiological parameters. Additionally, N_v in the expansion experiments was chosen as the value corresponding to the maximum areal coverage bin (Table 1), representing areas that have recovered to as dense a level as possible.

3 Results

Expansion scenario simulations were conducted for 2017 and subjected to monthly statistical analyses to determine the effects of seagrass expansion on hydrodynamics. The analyses are presented in the following subsections in terms of changes in the temporal mean and the 95th percentile for the month of October. These values indicate the seagrass's hydrodynamic engineering capacities on average and under extreme conditions.

3.1 Hydrodynamics

The effect of seagrass on sea level is not very high in the different scenarios. However, the effect is sufficient to result in different wetting and drying states between the scenarios, given that the critical threshold for water column to become dry (5 cm) is reached earlier or later depending on the scenario. Changes in the dry time ratio (i.e., the relative amount of time an area remains dry during the tidal cycle) potentially reach over 20% for the shallow littoral zone (not shown). Therefore, the calculations of the mean and quantile are based on the time an area remains wet within all scenarios and the respective time window varies in space.

3.1.1 Sea surface height

As initially mentioned, the effect of seagrass on sea surface height (SSH) is fairly limited and varies locally only within the range of a few millimeters to cenimeters when considering the average conditions (Figs. 4a and 5a). While the signs of changes are not necessarily the same everywhere, especially in the high-energy scenario in which seagrass occurs at the side of the channels, seagrass generally reduces the sea level where it is located (Figs. 4 and 5). This result is different for the situations where seagrass expands in very large mounts, such as in the Veg_{max} (E4) scenario; in this case, average sea level is reduced in the meadow itself, but increases in the adjacent unvegetated area.

For the upper 95th percentile (Figs. 4b and 5b), the situation tends to change to the opposite result, and the presence of seagrass broadly reduces the sea level height, which can be up to more than 15 cm or 10–15% for the maximum seagrass expansion scenario (relative changes are depicted in supplementary Figs. S3 and S4. There are exceptions where sea level increases in the EFWS in a few very shallow littoral areas towards the coast. In the scenarios with seagrass expansion in approximately 10% of the areas (E4:Veg_{LE}, E5:Veg_{HE}), the reductions are mostly in the order of a few centimeters. For the scenario with very large expansion (E3), with respect to the quantiles, sea level is reduced not only in the Wadden Sea but also in the adjacent regions (Figs. 4b and 5b).

3.1.2 Velocity magnitude

Compared to the changes in sea level, the effect of seagrass on current velocity (showing depth-averaged velocities here) is more pronounced (Figs. 6 and 7). Current velocity can be reduced within seagrass meadows by more than 10–30 cm/s (strongest reduction in the depth interval −1 to 1 m) compared to the same areas without seagrass (E2). This reduction is over 50% to almost 80% in relative terms (supplementary Figs. S5 and S6) with respect to the monthly mean. A reduction in the current velocity in response to the seagrass is observable within both the EFWS and NFWS.

The widespread decrease in current velocity is moderately countered by partially enhanced current velocity magnitudes within the seagrass-free tidal channels. This localised velocity increase predominantly occurs in the Veg_{max} scenario as well as to a lesser degree in the Veg_{HE} scenario with seagrass bordering the channels. Predominant examples for this are the channels north of Sylt in the NFWS and the channels next to Langeoog and Spiekeroog, in addition to Jade in the EFWS (Figs. 6 and 7). In the Veg_{LE} scenario, oceanward from the coastal seagrass meadows, where current velocity is attenuated, velocity also shows localised tendencies of minor increases.

The effects of additional seagrass, leading to overall reduced current velocity in the vegetated zones and localised increases in some tidal channels, are similarly observable on the difference maps of the 95% quantiles (Fig. 6b and to those of the averages Fig. 7b). However, while the spatial patterns in current velocity differences remain similar, the magnitude of the differences slightly increases. The differences in the quantiles indicate maximum current velocity reductions of 25 cm and more (up to 0.8 m) in the presence of seagrass, denoting similar relative changes compared to the changes in monthly mean velocity magnitude ($> 20\%$ and approaching more than 80% for the shallow most zones, supplementary Figs. S7 and S8).

Figure 8 depicts profiles of velocity magnitude, TKE, and bottom sediment concentrations in the East Frisian Wadden Sea simulated during storm Herwart on October 29th, 2017, which pushed water coastwards in the EFWS. During strong currents, such as maxima during flood and ebb, the presence

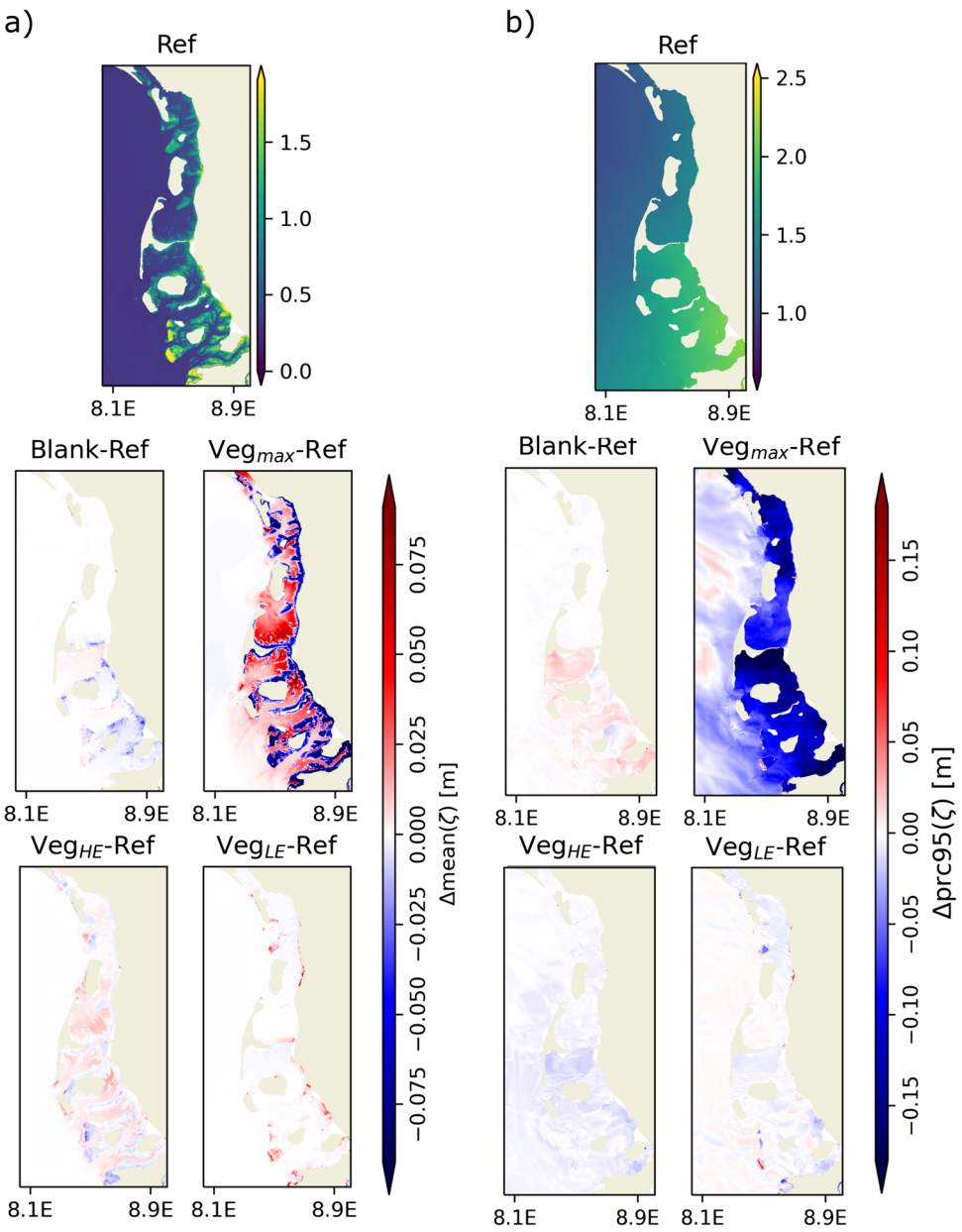

Fig. 4 Comparison of temporally averaged (**a**) and 95% quantile (**b**) of sea surface height in NFWS, showing from left to right values for reference and difference of scenarios (E2–E5) minus reference

of a seagrass meadow (P1, southeast of Borkum) reduces the current velocity (uneven rows) in the Ref scenario (blue curve) by up to 50% compared to the vegetation-free scenario (orange curve) during ebb (Fig. 8j) and flood situations (Fig. 8g).

As seagrass densities in the remaining seagrass scenarios further increase, assuming a population increase for this meadow and in general (Table 2), current velocity is dampened further (purple, red, and green lines (purple and red are overlapping)). Comparing the scenarios in an unvegetated location (Blank) in the tidal channel west of Borkum Island (Fig. 8, P0, a, d), differences between the scenarios remain widely unnoticeable during flood except for the scenario Veg$_{max}$ (green curve). In this scenario, the enormous presence of seagrass leads to increased velocity during flood currents (Fig. 8a) and decreased velocity during ebb currents (Fig. 8d).

3.1.3 Bottom stress magnitude

Consistent with the results for current velocity, the largest bottom stress values occur within the tidal inlets and along the tideways where velocities are high. For the NFWS, monthly averages amounted to approximately 0.8 Pa and the quantiles to approximately 2 Pa (Fig. 9) with similar values in the EFWS for the Ref run (supplementary Fig. S7). Towards the

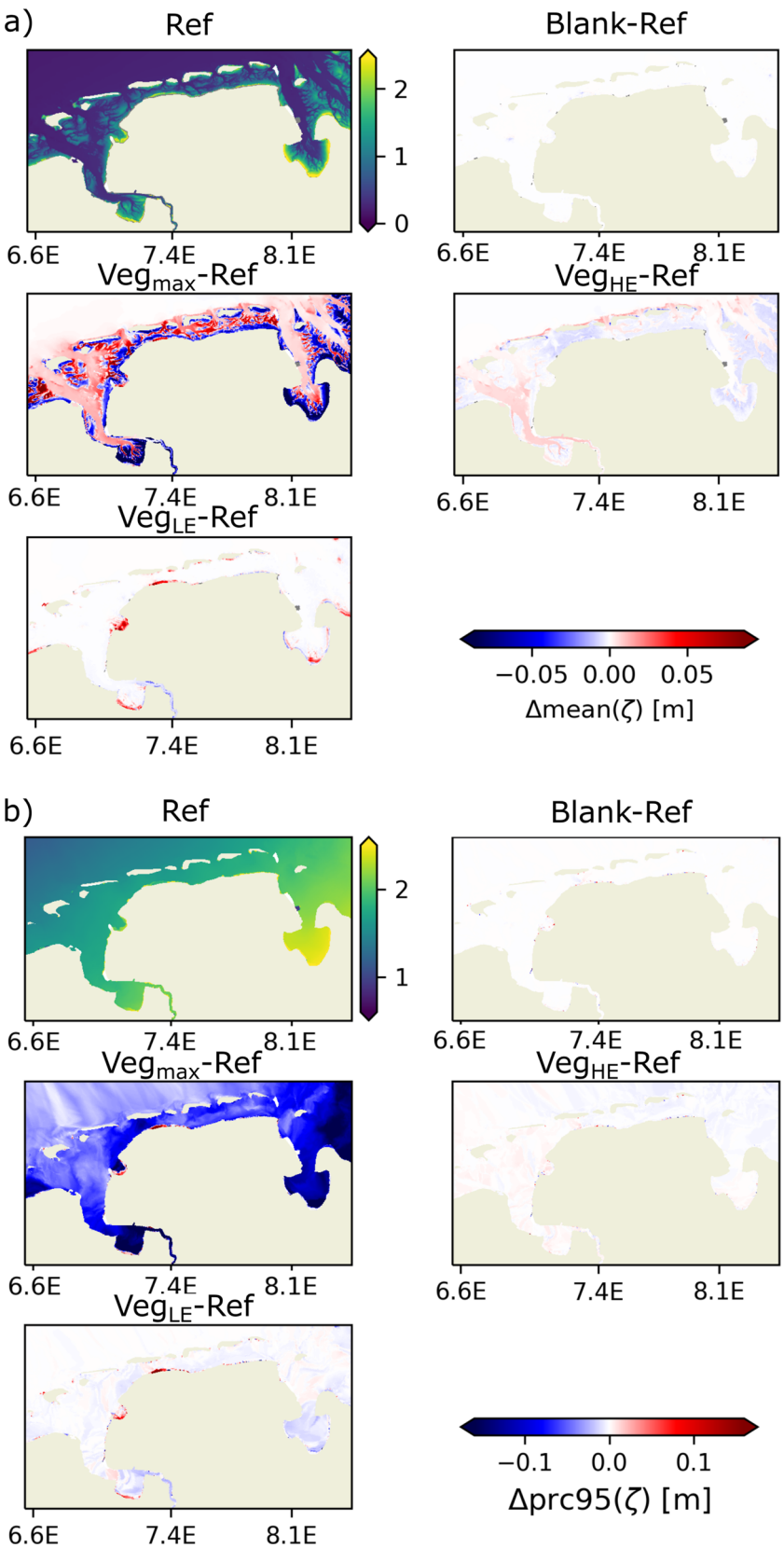

Fig. 5 Comparison of temporally averaged (**a**) and 95% quantile (**b**) of sea surface height in EFWS, showing from left to right values for reference and difference of scenarios (E2–E5) minus reference

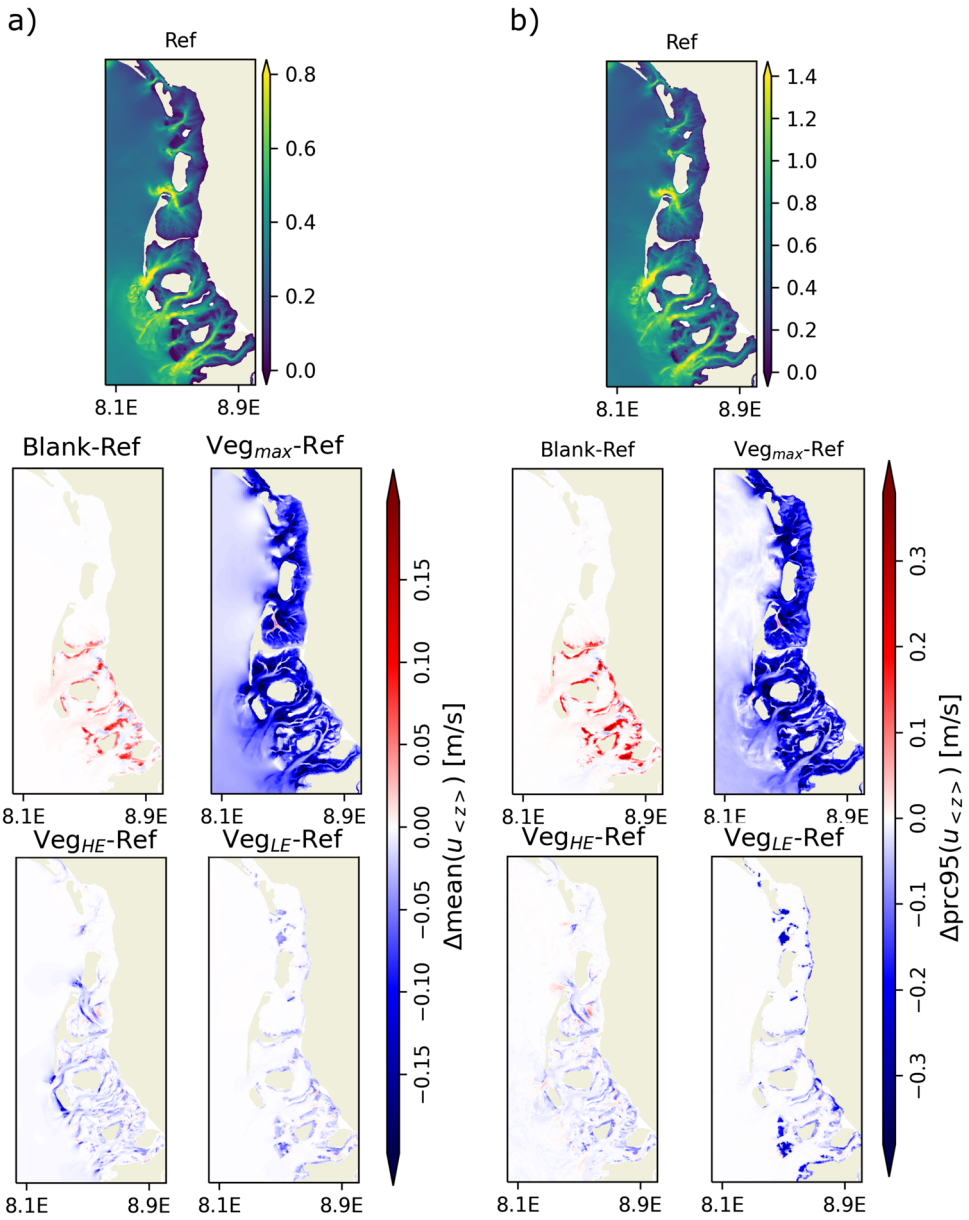

Fig. 6 Comparison of temporally averaged (**a**) and 95% quantile (**b**) of depth-averaged velocity in NFWS, showing from left to right values for reference and difference of scenarios (E2–E5) minus reference

tidal flats and supralittoral zone, the bottom stress average and quantiles decrease to values below 0.4 Pa, approaching zero.

The presence of seagrass bounding the islands in the southern half of the NFWS dampens the velocity, consequently leading to reduced shear stress. In the absence of seagrass (Blank run), the shear stress was higher on average by 0.1 to 0.3 Pa (Fig. 9 second from left panel), which is more than 50%. Similarly, in the EFWS at the dense seagrass bulge southeast of Borkum, the average bottom shear stress was higher by up to 0.25 Pa in the absence of seagrass. The introduction of additional seagrass in the scenarios Veg$_{HE}$ and Veg$_{Le}$ has a similar impact on the newly recovered areas. Negative differences are higher in the Veg$_{max}$ scenario, where the local attenuation in velocity added up, such that on average, maximum stress reductions of 0.3 Pa or more are found. This velocity reduction consequently leads to reduced shear stress, even outside the Wadden Sea area.

For the Veg$_{max}$ scenario, which covers the entire seagrass depth range, the relative reduction in the 95th percentile of bottom stress range from approximately 25 to 59% between depth of 3 and 4 m, 25 to 80% between depths of 3 and 2 m, and approach almost 100% in the shallower areas (Supplementary Fig. S10).

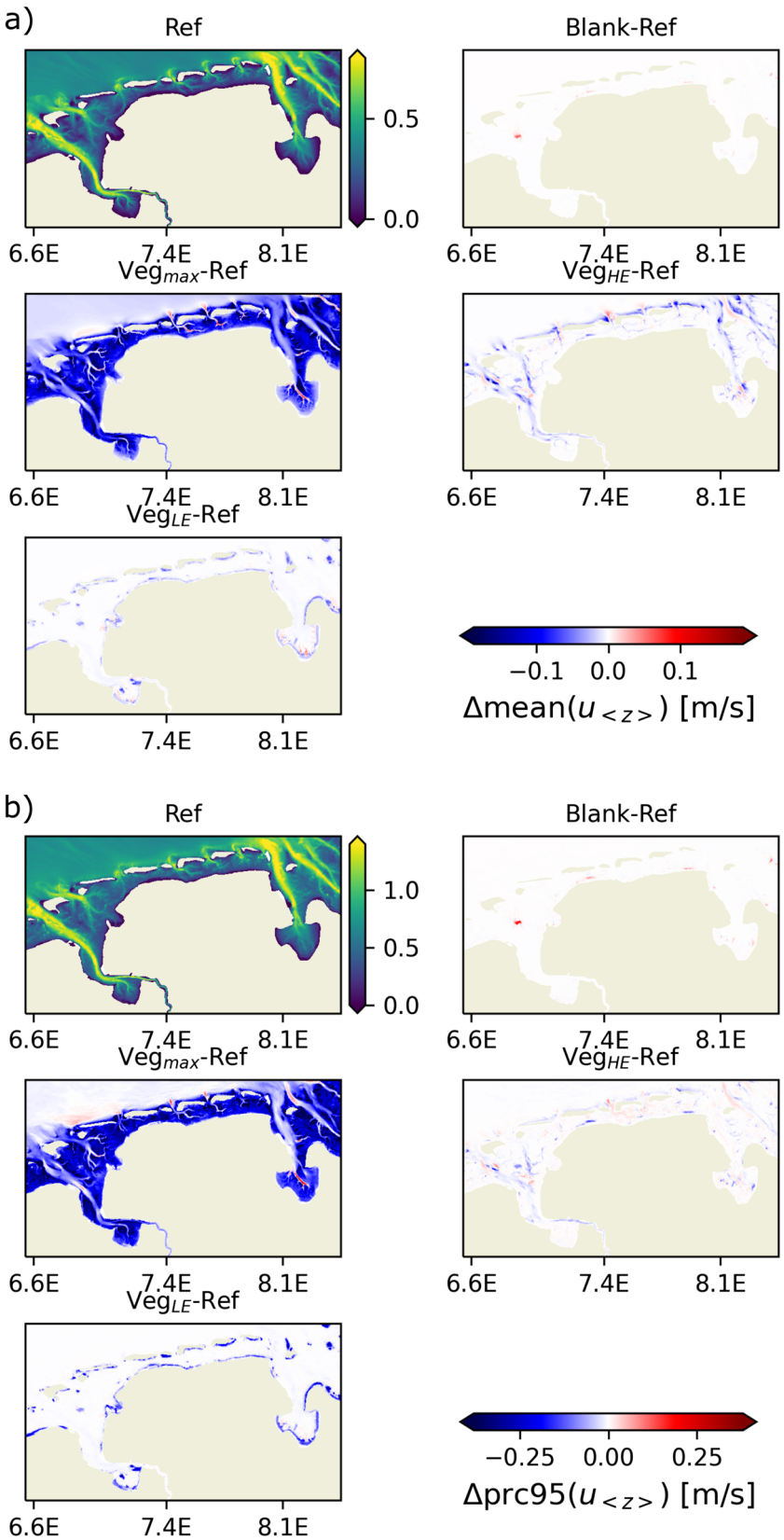

Fig. 7 Comparison of temporally averaged (**a**) and 95% quantile (**b**) of depth-averaged velocity in EFWS, showing from left to right values for reference and difference of scenarios (E2–E5) minus reference

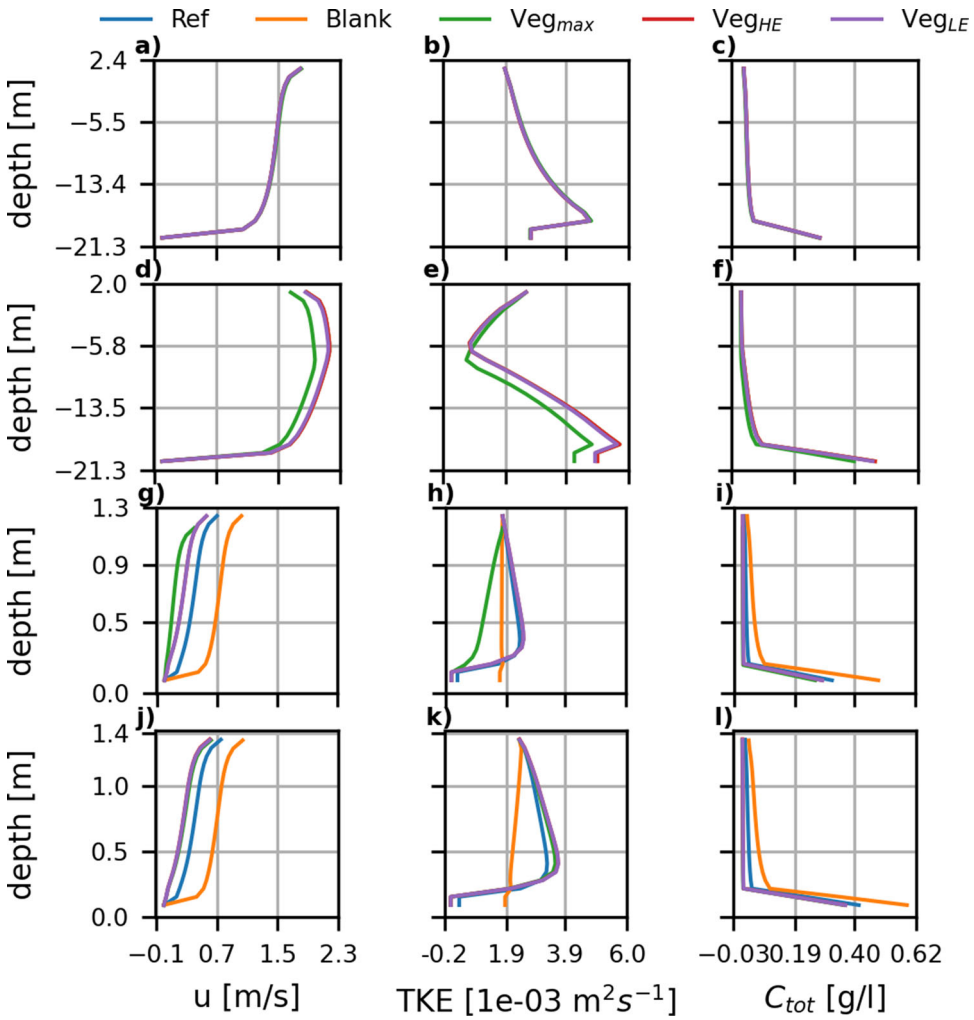

Fig. 8 Profiles of velocities and total SPM concentrations (alternating from top to bottom) during maximum flood (**a**–**f**) and maximum ebb (**g**–**l**) at point P0 (left column) in the inlet west of Borkum and the seagrass meadow south of Borkum P1 (right column). Different seagrass scenarios are encoded in line colours

3.2 Turbulent kinetic energy

The effect of seagrass on the distribution of turbulent kinetic energy (TKE) in the water column is shown in Fig. 8b, e, h, and k. At the Borkum seagrass meadow (P1), during strong flood and ebb currents (Fig. 8h, k), the vertically relatively uniform distribution of TKE in the scenario without vegetation (orange) is altered towards strongly reduced values (an order of magnitude) in the bottom boundary layer in the Ref scenario, which introduces 'actual' summer seagrass distributions (blue curve).

However, TKE in the Ref scenario is enhanced above a depth of 0.2 m (positive values denote dry at undisturbed sea level), which is slightly on top of the upper canopy layer (leaf heights of 14 cm are used and measured from the respective bottom). The increase in the Ref scenario is approximately a factor of 1.5 during the maximum ebb and approximately a factor of 1.3 during the maximum flood current. For the other scenarios, where the local seagrass meadow is denser, the decrease in the bottom layer and the increase in the above-canopy layer and towards the surface are slightly enhanced. The only exception is the $\mathrm{Veg_{max}}$ scenario, where the dampening over large areas alters the current velocity more strongly, leading to a decrease in flood current and a later development of the maximum flood current in the meadow.

Therefore, the large-scale dampening effect is stronger than the local effect of that one meadow alone. The TKE in the channel (P0) remains generally unchanged in all scenarios (Fig. 8b, e), except in the Veg_{max} scenario. In the $\mathrm{Veg_{max}}$ scenario, TKE responds to the increased flood and reduced ebb velocities in the channel due to the previously mentioned increased channelisation effects in response to the increased resistance to flooding and drainage of the tidal flat areas.

The increased protection of the bottom layers due to denser vegetation increases turbulence generation above the canopy, as shown in Fig. 8. This effect is observed in all expansion areas. The increased protection leads to a reduction of more

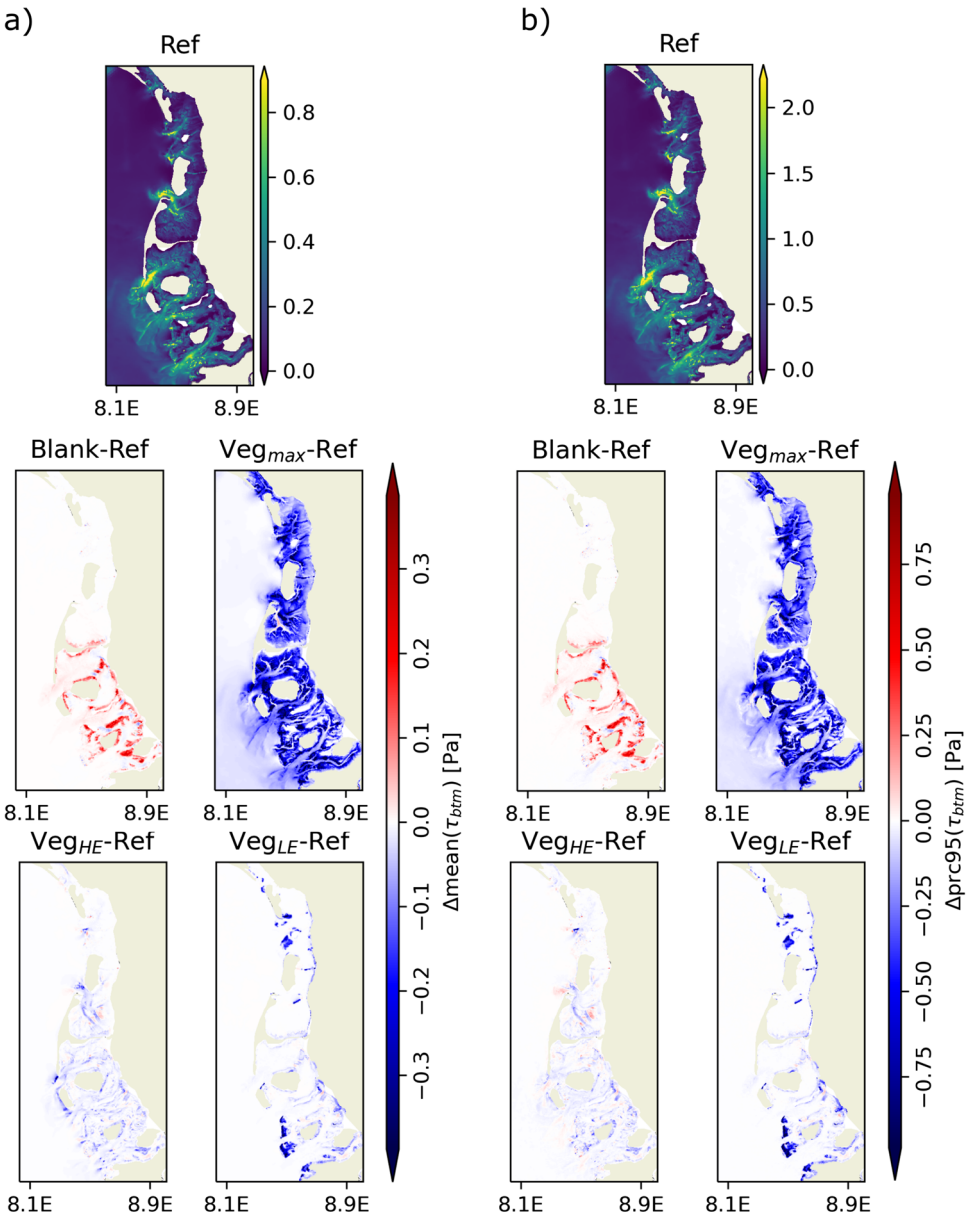

Fig. 9 Comparison of temporally averaged (**a**) and 95% quantile (**b**) of bottom stress in NFWS, showing from left to right values for reference and difference of scenarios (E2–E5) minus reference

than 75% in the average and quantile of bottom TKE in the shallower meadows, and 30% in the deeper vegetated regions (Fig. 8e, supplementary Figs. S10 and S11). In the adjacent channel and tidal flat area, there is a reduction of a few percent points. Towards the surface, the difference in TKE becomes extremely small, at less than 1% (not shown), as is indicated by the profiles.

3.3 Wave dynamics

Significant wave heights (HS) approaching the barrier islands equal approximately 1 to 1.5 m in terms of the monthly average, and the 95th percentile of significant wave heights is approximately 1.5 to 2 m (Figs. 10 and 11). As the waves enter the back barrier Wadden Sea, wave heights decrease as the shallow bathymetry promotes wave breaking and friction. This results in HS decreasing to below 0.5 m and approaching 0 m. The presence of seagrass (Blank-Ref) contributes to wave attenuation, additionally reducing HS by a few centimeters up to more than 20 cm on average, and over 40 cm locally with respect to the quantiles. The seagrass expansion scenarios indicate a further reduction of a few centimeters in the shallow areas and reductions of over 40 cm on average and over 60 cm with respect to the 95th percentile for the locations where seagrass would occur in deeper areas where still relatively high waves occur. Where seagrass occurs, it generally reduces HS by over 20% in the deeper areas and by more than 50% in regions shallower than 1 m. In the shallowest regions that are still vegetated, waves are almost completely attenuated.

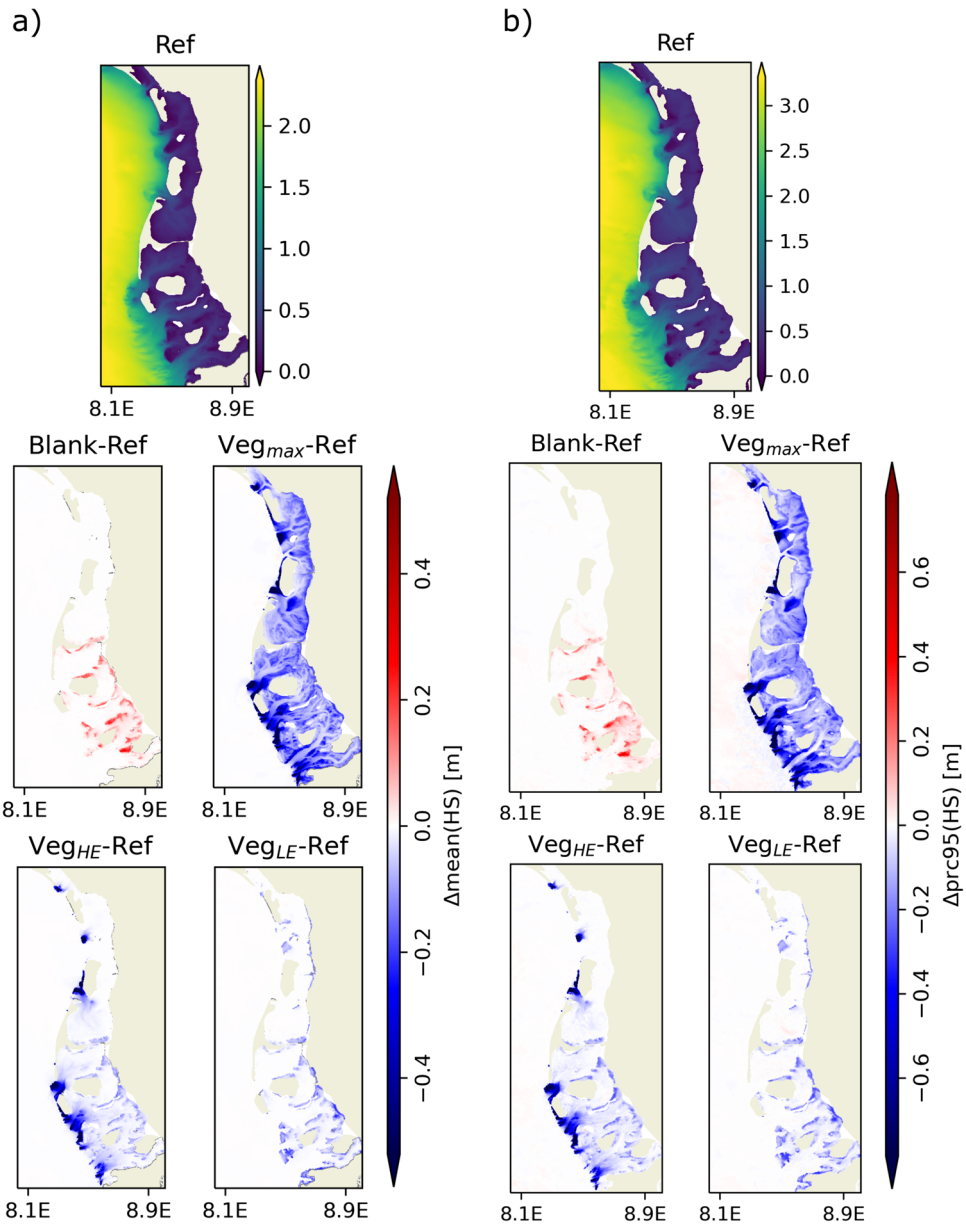

Fig. 10 Comparison of temporally averaged (**a**) and 95% quantile (**b**) of significant wave height in NFWS, showing from left to right values for reference and difference of scenarios (E2–E5) minus reference

3.4 Sediment dynamics

The sedimentation budget depends on the balance between erosion and deposition. Erosion occurs when the critical shear stresses of the sediment type are exceeded, mobilising sediment and suspending it in the flow, allowing for transport away. On the other hand, deposition happens when formerly suspended particles (eroded elsewhere) sink to the bottom due to insufficient turbulence, ultimately succumbing to gravitational pull.

Erosion is typically at its highest point when the greatest shear stress occurs in response to peak current velocities. In addition to the previously discussed current velocity profiles for a location in the channel and the seagrass meadow near Borkum, Fig. 8c, f, i, and l shows the corresponding profiles of total suspended sediment concentrations integrated over all 8 sediment classes. Related to the changed velocity profiles in response to the presence and increased density of seagrass (Fig. 8, first column), total suspended particulate matter (SPM) concentrations (Fig. 8c, f, i, l), are reduced by approximately 30% (approximately 0.2 g/L) in the bottom layer and relatively more in the layers above, basically diminishing the upward transport in the water column for the most dense seagrass meadows (P1, i, l).

At the channel location, scenario-induced changes to the local sediment profile are limited to the Veg$_{max}$ scenario (E4), where a significant SPM reduction in the channel can be seen for the profile at maximum ebb current, as overall less mate-

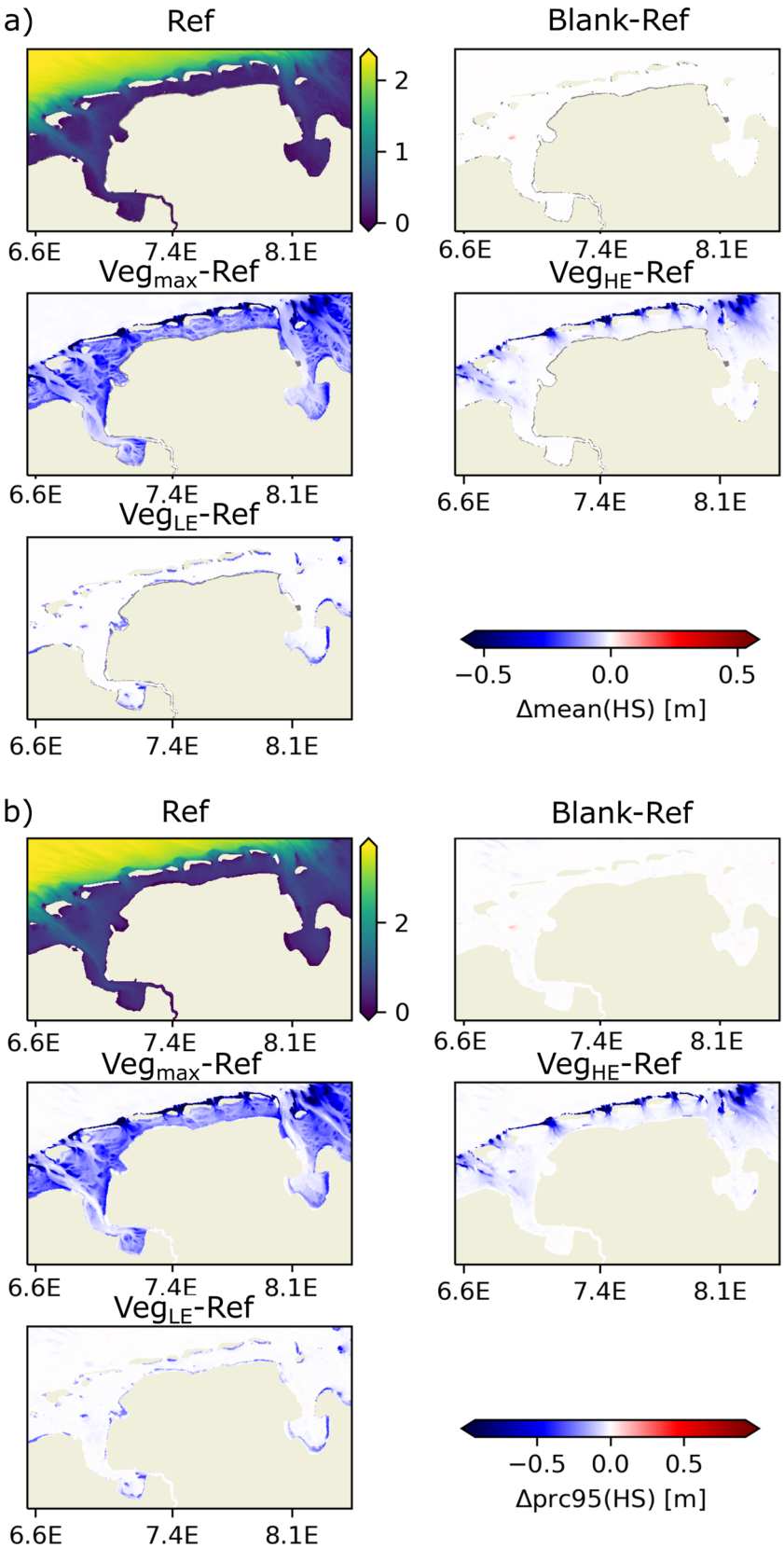

Fig. 11 Comparison of temporally averaged (**a**) and 95% quantile (**b**) of significant wave height in EFWS, showing from left to right values for reference and difference of scenarios (E2–E5) minus reference

rial from the large-scale flat areas is eroded and transported into the channel.

In the Wadden Sea areas, the reduced stress at the bottom leads to a reduced mobilisation of sediments, which is reflected by decreased/increased monthly average bottom concentrations on the order of a few centigrams per liter to maximum decigrams per liter, in the presence/absence of seagrass (Figs. 12a and 13a). This is a reduction locally by over 30% compared to the Ref scenario.

During strong current conditions, sediment mobilisation, as indicated by the 95th quantiles, is reduced by up to more than half a gram per liter (Figs. 12b and 13b). However, smaller increases in the areas neighbouring the recovery areas are present and are related to the smaller increases in current velocity and bottom stress.

In the shallow intertidal zone below 0 m, the sediment concentration almost reaches 0 g/L, showing strong reductions of up to 2 g/L in the 95th percentiles during the storm period (supplementary Fig. S9). Changes in average SPM concentrations at the surface (supplementary Figs. S12 and S13) match the pattern of those at the bottom, demonstrating a strong decrease in concentrations due to vegetation.

However, for the quantiles of SPM locally and in the EFWS, especially Jade Bay, an opposing trend of increased surface concentrations for the Veg_{LE} scenario occurs.

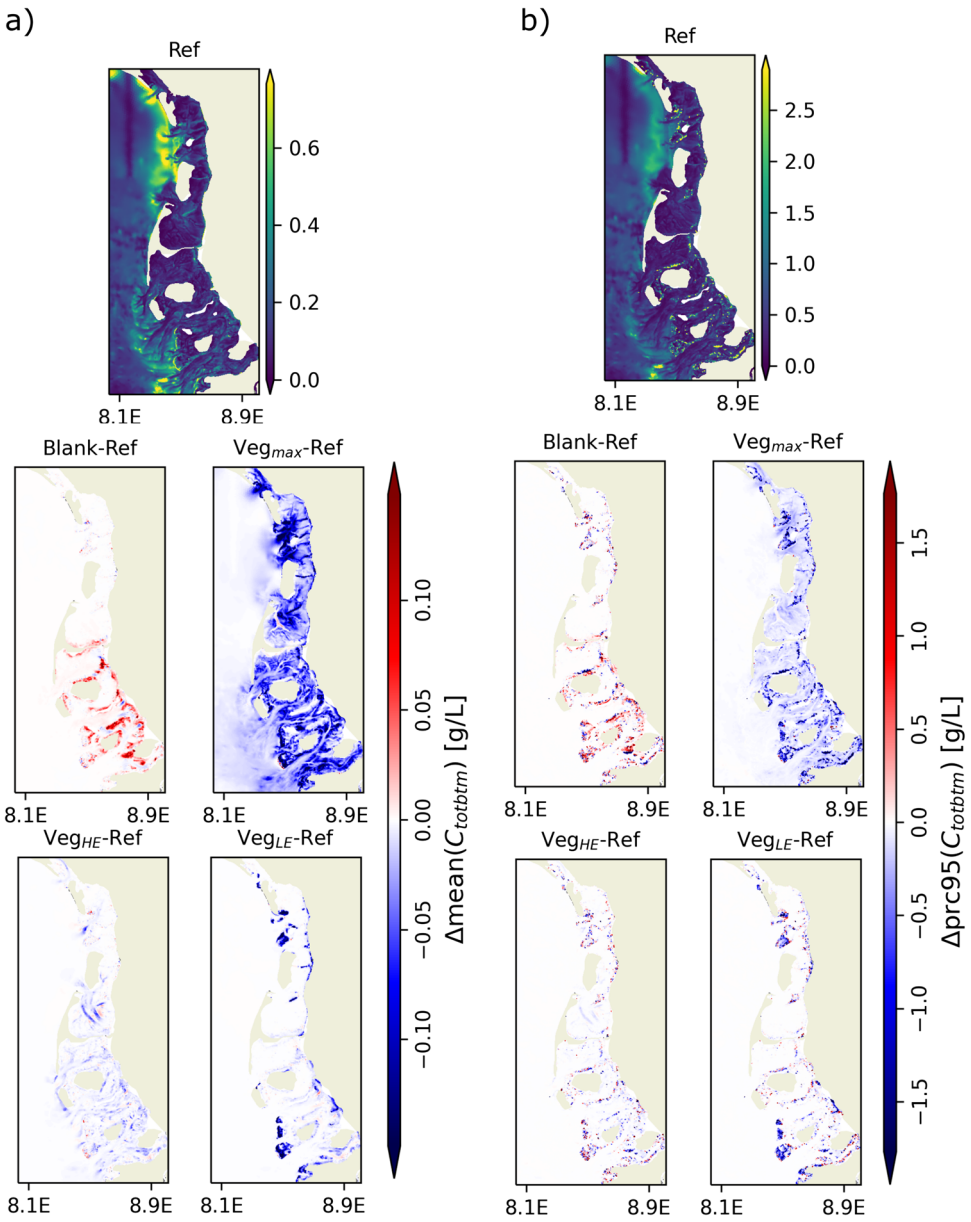

Fig. 12 Comparison of temporally averaged (**a**) and 95% quantile (**b**) of total SPM concentration near bottom in NFWS, showing from left to right values for reference and difference of scenarios (E2–E5) minus reference

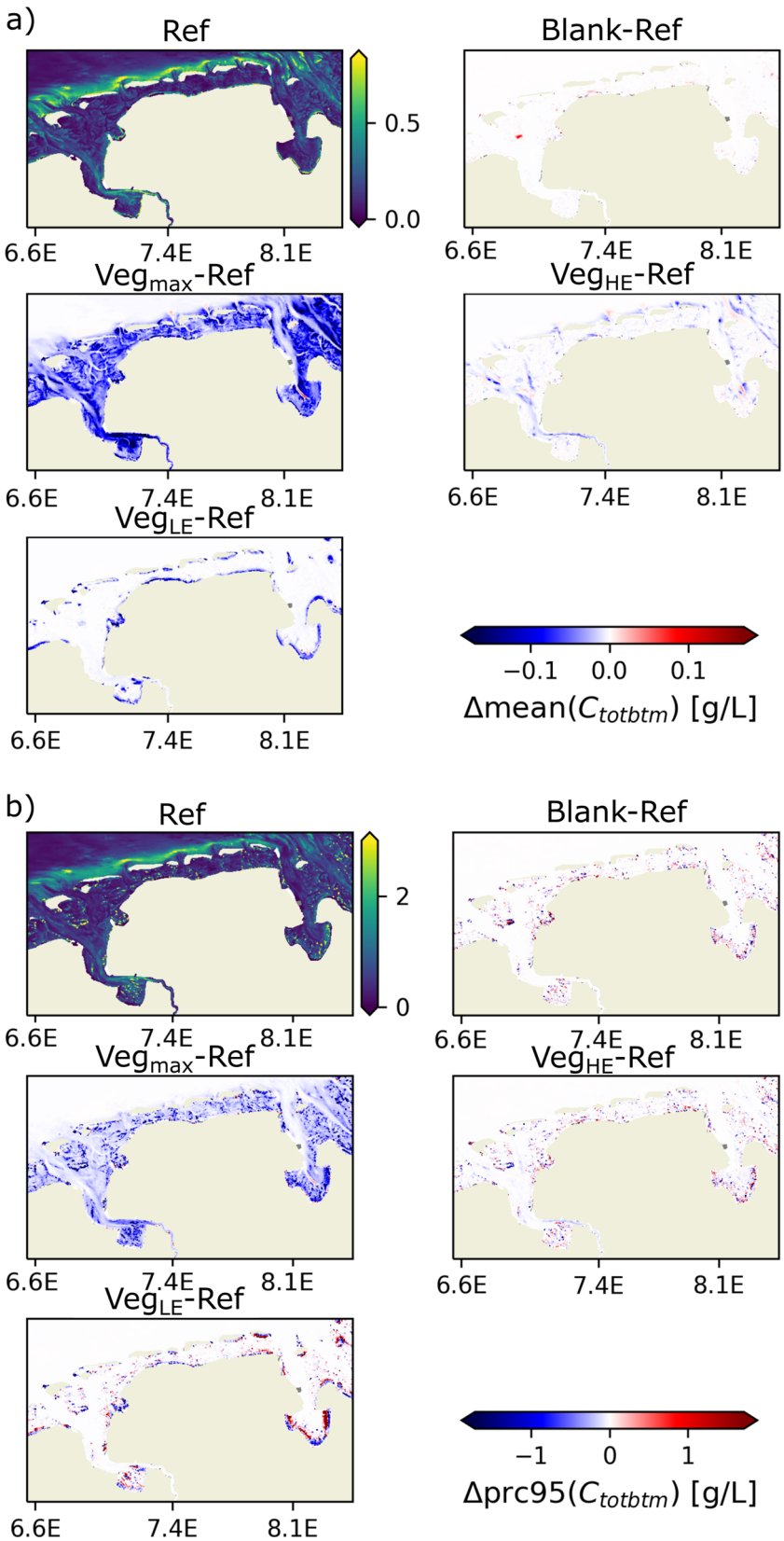

Fig. 13 Comparison of temporally averaged (**a**) and 95% quantile (**b**) of total SPM concentration near bottom in EFWS, showing from left to right values for reference and difference of scenarios (E2–E5) minus reference

3.5 Impact on different variables

Our experiments generally suggest that the introduction or increase of seagrass leads to a significant reduction in the magnitude of most variables (Sects. 3.1–3.4) ranging from 20% to over 90% for the deeper and shallower vegetated zones, respectively. This result is the same for both the monthly average and 95th percentile, when introducing or increasing the amount of seagrass.

For current velocity, the reductions were of typically a few centimeters per second to diameters per second, with a maximum of up to 0.5 m/s in mean values of depth-averaged velocities and quantiles for the densely vegetated zones. HS shows quantile reductions of a few centimeters, depending on the scenarios, with an average reduction of 10 to 25 cm. Maximum reductions of up to 0.4 cm are found near a depth of 0 m, and isolated reductions above 1 m occur when seagrass is located in the deep intertidal area and thus exposed to higher wave heights.

Ranking the variables based on the relative reduction of monthly mean values within the Borkum meadow (comparing the scenarios Ref and Blank), the strongest reductions (in all cases above 80%) are observed for the variables (in descending order): bottom stress, bottom TKE, bottom layer SPM concentrations. In contrast to the other variables, TKE also significantly increase above the canopy layer. Depending upon the scenarios compared, the next most dampened variables are the depth-averaged velocities ($\sim 50\%$ reduction from Blank to Ref). For the expansion scenarios compared to Ref, however, the additional dampening is significantly stronger for significant wave height ($> 80\%$) from Blank to a scenario incorporating a denser seagrass meadow. For the sparsely populated seagrass meadow (Ref), the reduction only amounts to $> 30\%$. However, these strong responses do not occur in the sea surface height levels. While the 95th percentiles minimally decrease (a few centimeters), the monthly averages are partially increased in response to seagrass. For large seagrass amounts (Veg_{max}), there is a tendency for the average water level to increase in front of the vegetated zone and to decrease within the zone.

3.6 Contrasting the experiments

The scenarios generally confirm that an increased vegetation density and spatial extent of seagrass coverage lead to an increased attenuation capacity and reduced erosive potential of currents, as momentum dissipation accumulates.

Among the scenarios, Veg_{max} is the only one that notably affects SSH, reducing the 95th quantile by up to more than 10 cm. Within the meadows, average reductions of a few centimeters are found, while in the adjacent channel areas, a slight increase of a few millimeters to centimeters in water level is found. As the highest current velocities appear along the tidal channels and deep tidal flat areas, the Veg_{HE} scenario was set up introducing seagrass where erosive potential is the highest and hypothetically a larger amount of energy could be absorbed. Compared to the Veg_{LE} scenario, this indeed locally led to higher attenuation in absolute values of currents and waves. Reductions in HS approaching and succeeding 0.5 m are only reached within scenarios Veg_{HE} and Veg_{max} (Fig. 10), where seagrass is still exposed to higher wave heights.

While the expansion of seagrass leads to an in situ reduction in current velocity magnitude, scenarios introducing a substantial amount of seagrass at the tidal flat areas bordering the channels (E3, E4) show the opposite effect of an increasing velocity magnitude, which is partially observed within the adjacent vegetation-free tidal channels (Fig. 7).

The highest reductions in bottom layer sediment concentrations are typically found in the shallower areas that are covered by seagrass in the Veg_{LE} and Veg_{max} scenarios (Figs. 12a and 13a).

In addition to the introduction of seagrass in additional areas, the stem density in already covered areas was increased in scenarios E3-E5, reaching a maximum of 7360 stems/m^2. Comparing scenario E1 to E4 in the inner part of the meadow located near Borkum in the EFWS, the reduction in monthly average and 95th percentile compared to E2 increases from 34 to approximately 85% and from 23 to 77%, respectively. Reductions in depth-averaged current velocities for the monthly mean (0.31 m/s) and 95th percentile (0.48 m/s) without vegetation were reduced by 76% and 69%, respectively, compared to 49% and 48% for the Ref scenario, respectively.

While the reduction in significant wave height and depth-averaged velocities increased significantly in relative terms with further increases in vegetation density (E3–E5), the reduction in bottom stress, TKE, and total suspended particulate matter within the meadow is already high for a sparser seagrass population (E1), with reductions of the average and quantiles exceeding 80–90% compared to E2. Further increasing the density to the upper limit of 7600 shoots per m^2 (as in scenarios E3-E5) increases the relative reduction by up to 99% for both quantiles compared to E2.

3.7 Contrasting severe and calm weather

In order to compare the effectiveness of attenuation during severe and calm weather, two tidal cycles (from October 28th until October 30th) during the storm event have been compared to the tidal cycles 10 days prior to the storm (October 18th–October 20th) based on the previous statistical measures (mean and 95th percentile).

Overall, with the increased values observed in the hydrodynamic values during the storm, the (predominant) attenu-

ation due to the seagrass also increases in absolute values. The relative reductions compared to the realistic scenario with sparse seagrass (Ref) remain relatively similar for the variables, significant wave height, bottom stress, TKE, and SPM concentrations. For these bottom-referenced variables, relative reductions of over 90% are found in the areas shallower than 2 m, and decreases of over 10% occur within the areas up to 4 m depth for the Veg_{max} scenario (supplementary Fig. S11).

4 Discussion

In the preceding section, the effects of extended seagrass amounts and areas on various hydrodynamic, wave, and sediment parameters were demonstrated. In this section, the results will be discussed in the following with respect to our research questions:

4.1 Results for our research questions

4.1.1 Impact on different variables

Research question (I) focuses on the reduction of current and wave strength by seagrass, as well as the impact on different variables in general.

The changes in the averages and quantiles of SSH (Sect. 3.1.1) due to seagrass amounted only to a few percent (few millimeters to centimeters); for the other analysed variables (Sects. 3.1.2–3.4), the change in magnitude overall varied between the different parameters. The results in general suggested a significant reduction in the relative magnitude of between 20% and over 90% for the deeper and shallower vegetated zones, respectively. The higher attenuation in the shallow areas can be attributed to the contribution of the shallow bathymetry via frictional damping and depth-induced reduction of wave energy by wave breaking, such that small magnitudinal changes induced by seagrass become larger in relative terms compared to a similar reduction in the deeper parts, where current velocities and wave heights are still higher.

The quantiles of depth-averaged current velocities and wave heights have been reduced by up to more than 0.5 m/s and 1 m, respectively. Since the bottom drag coefficient is proportional to the square of the above boundary layer velocity magnitude, and velocity reduction is strongest within the vegetation layer, the effective reduction seen in the velocity translates to a considerably large and potentially even greater relative reduction in bottom stress magnitude (up to over 1 Pa in 95th percentile).

Therefore, erosion is reduced and the duration of settling conditions is enhanced, favouring sedimentary conditions and leading to reduced concentrations of bottom layer total suspended particulate matter. This reduction is reflected by the overall strongly, and in the shallow meadows almost completely, reduced concentrations of bottom layer total SPM load, which for the 95th percentile can reach up to 2 g/L.

The highest relative reductions were observed for the bottom-referenced variables, including bottom stress, bottom SPM, and bottom turbulent kinetic energy (TKE). These variables experienced the most significant reductions due to the limited drag effect of the vegetation layer, which extends only to the submerged part of the water column. The increase in TKE above the canopy layer (20 cm) is a response to the velocity shear within the vegetation zone and generation of TKE due to the flow interactions with the canopy.

As sea level changes are balanced by the vertically integrated flows, and spatially more homogeneous, they are impacted the least. Overall, the kinematics are damped quite effectively, while the impact on surface fluctuations is much weaker, though significant wave height is significantly reduced in relative terms as well. This overall illustrates that seagrass is an effective NbS for erosion reduction but has limited direct use for flood protection.

4.1.2 Contrasting the experiments

Research question (II) focuses on the impact of the different seagrass positioning and in particular on comparing the effects on hydrodynamics between sparser and more densely populated seagrass meadows.

In general, the recovery of seagrass in deeper intertidal areas and closer to the channels allows for interaction with larger current velocities and waves, resulting in stronger attenuation in absolute terms. For erosion protection, larger meadows in shallow regions were found to be most effective.

However, the recovery of seagrass in deeper intertidal areas bordering the tidal channels can have opposing effects, leading to an increase in current velocity in parts of the channel. This effect is mainly observed during coastward currents, where the increased flow resistance in the vegetated areas sets up water levels in the channels, enhancing channelisation effects. The decreased resistance in the channel relative to the seagrass meadows makes the channels a more favourable pathway for the water masses piling up in front of the seagrass meadows. Consequently, water levels in front of the seagrass meadows can also increase.

While the effect of hydrodynamics on seagrass is not considered here, the reported higher survival rates for large patch recoveries (Irving et al. 2014; Gagnon et al. 2021), and higher survival rates under low energy conditions, highlight that the presented Veg_{LE} scenario is most realistic in terms of introducing resilient seagrass populations.

Using the example of the Borkum meadow, it was demonstrated that even a sparse configuration of the meadow (a few hundred shoots per m^2, REF) effectively dampened sediment

concentrations and shear stress in the bottom layers, with reductions of more than 80% on average. As the shoot density increased towards the recovery scenarios, approximately tenfold, the vegetation drag term increased accordingly. This led to further increases in attenuation of $\sim$ 13% and $\sim$ 14% for these two variables, respectively. The attenuation of depth-averaged currents and significant wave heights increased by approximately 25% and 50%, respectively, in addition to the reductions of $\sim$ 49% and $\sim$ 34% seen in the REF scenario compared to the vegetation-free scenario. These results indicate that a denser seagrass coverage has a greater effect on the dynamics than a sparser meadow configuration.

4.1.3 Contrasting the EFWS and NFWS

Research question (III) focuses on the similarities and differences between the EFWS and NFWS. Generally, the analysis of the different numerical experiments demonstrated very similar results for both areas. This stems from the fact that both systems are subject to similar physical conditions as multitidal inlet systems in a meso- to macrotidal environment with significant wave incidence. However, there are some marginal differences between the two areas. Tidal amplitudes are slightly higher in the EFWS compared to the NFWS, and the dominant wind direction is SW, favouring higher waves in the NFWS compared to those in the EFWS. The most significant difference between the two areas is the much larger presence of seagrass in the NFWS compared to the EFWS. As a result, there is already a significant impact of seagrass on coastal hydrodynamics under present-day conditions. In contrast, in the EFWS, there is hardly a difference between scenarios without seagrass (Blank) and with the realistic seagrass distribution (Ref), except for the one seagrass meadow near Borkum island. Considering the strong dampening effect of seagrass on coastal kinematics, increasing seagrass coverage in the EFWS to the level observed in the NFWS would already represent a significant progress.

4.1.4 Contrasting severe and calm weather

Research question (IV) addresses whether the accumulative effect during calm weather periods is more important than the attenuation provided during extreme events with respect to erosion and flooding risks. The results of the model indicated an increase in attenuation in absolute values when comparing extreme conditions to calm weather conditions, with a minor decrease in the relative amount. These results on their own suggest that seagrass impacts are slightly stronger under extreme weather conditions. However, this result does not take into account the model limitations (further discussed in Sect. 4.3). The reduction in SPM concentrations, which are used as a proxy for reduced erosion, are already quite high, amounting to relative values of 90% in the vegetated meadows. It is important to consider that by the time most storms occur, the seagrass population is already almost absent due to the seasonal vegetative cycle and accumulated storm damage. Additionally, regarding extreme events occurring during vegetated periods, for simplicity purposes, the majority of the seagrass population is assumed to occur in a 1:1 ratio of *Z. marina* and *Z. noltei*. As generally the physiologically smaller *Z. noltei* is more abundant, this in addition to the overall sparse population density further limits the attenuation potential of seagrass corresponding to the observable present-day status.

Because seagrass has a negligible direct impact on sea level, and the wave attenuation is spatially limited, due to the relatively narrow widths of the vegetated zones and their distance from dikes, seagrass areas provide minimal protection against wave generation and amplification in the areas in front of the dyke.

However, taking into account the strong effect of bathymetry on fluid flow and waves, the effect of accumulating sediment to support the vertical height growth of the tidal flats appears particularly important for future sea level rise projections and is the main contribution expected from seagrass in terms of coastal flood protection.

While seagrass reduces sediment mobilisation and favours settling conditions, seagrass meadows predominantly accumulate fine sediments, and large amounts of what can be accumulated can be eroded relatively easily during winter storms when there is no seagrass left. However, the accumulated volume can act as an additional buffer and further consolidate depending on the amount and severity of storms.

4.2 Agreement with literature

Generally, scientific literature broadly supports the concept that seagrass has the potential to strongly dampen currents and short waves (Paul et al. 2012; Temmerman et al. 2023).

Reported attenuation rates of waves in seagrass/kelp beds that are close to 36% (Ferrario et al. 2014) are partially matched by relative reductions in quantiles and averages, seen in the deep part of the intertidal. However, in the shallow areas below 1 m depth, relative reductions begin to surpass 50% and approach 100% towards the shallow end of the vegetated intertidal zone (-1 to -2 m). This amount of reduction partially indicates an overestimated attenuation in the model results that is partially explainable by the low reference values for the relative differences, as the shallow bathymetry already very strongly dampens the incoming waves.

Furthermore, in reality, seagrass affects both the shear stress (Hansen and Reidenbach 2013) and the critical shear stress necessary to erode sediments, the latter of which is due to the stabilizing effect of the seagrass roots and rhizomes on the bed sediment (Christianen et al. 2013). The impact on critical shear stress (i.e., increased retention by parts of the plant

body) is not represented in the available sediment model. Observations suggest that bottom stress can be reduced by up to a factor of four (Hansen and Reidenbach 2012), and the critical shear stress can be reduced by a up to factor of two (Amos et al. 2004).

The relative changes in the individual model points in the scenarios greatly exceed those numbers, and given the shallow zone attenuation, the changes correspond to a reduction by factors in the hundreds.

Studying flows and particle trapping in the presence and absence of *Posidonia oceanica* (its leaf can be $\approx$ 10 times longer than those of *Zostera*) based on in situ observations in the western Mediterranean Sea, Gacia et al. (1999) confirmed that seagrass reduces current velocities proportionally to the height of the plant canopy, which is in line with the results of previous studies. They also found reduced amounts of particles trapped within the seagrass bed, indicative of a slight increase in particle trapping, and they found no linear correlation between trapping capacity and plant surface area, which is a strong argument for the importance of other factors such as bending. From their data-derived model, they found the retention capacity of the *P. oceanica* meadow to surpass that of an unvegetated bottom by a factor of up to 15.

This result is qualitatively in line with the overall effect in the simulations in this study that show that within seagrass meadows, averages and 95th quantiles of SPM concentrations are extensively decreased.

However, while seagrass beds primarily act as areas of net sediment deposition, Adams et al. (2016) in their meta-study also gathered evidence for opposing cases where an enhancement of turbulence can increase sediment resuspension (Lawson et al. 2012; Hansen and Reidenbach 2013).

Finally, the much lower responses of sea level to seagrass and the tendency to increase the sea level in front of its meadows are in agreement with the results of similar studies (Pillai et al. 2022). The effect tends to be negligible since, as in our case, plant heights are often small compared to the height of the water column.

4.3 Limitations of the model study

While the results indicate effective attenuation of kinematics in the vegetation zone, overestimation trends are apparent, and for the interpretation of the results, the limitations of the model approach and experiment implementation have to be considered:

First, the vegetation and flow interactions are unidirectional, with seagrass affecting the flow via turbulence and friction with a dependence of Z. Generally, in the presence of strong tidal currents, such as in the German Bight, the effectiveness of seagrass in terms of wave attenuation is reduced. This is because seagrass bends within the flow (Paul et al. 2012), reducing both its vertical extent in the water column and thus limiting its interaction with the larger wave orbitals, and the energy absorbed via horizontal vibrations of the plant body. As in our model, seagrass stems are modelled as rigid elements, the effect of bending is not considered, and in addition to the wave attenuation, the current attenuation is overestimated: In reality, drag would be reduced via the removal of the obstacle (i.e., the plant body) from the upper layers, leading to a decreased resistance of flexible plant bodies compared to that of solid obstacles. While this is certainly a significant simplification that does not capture the full complexity of seagrass dynamics, it is still a common simplification that enhances computational efficiencies facilitating model studies addressing larger temporal and spatial scales. Addressing the rigid cylinder approximation in laboratory and numerical studies, Vargas-Luna et al. (2016) concluded that using the rigid cylinder approach, numerical models are capable of representing the effects of high-density vegetation.

Moreover, the model simulation introduces seagrass once and only considers the effect of seagrass on the flow. It does neither account for the effect of flow on seagrass nor the biology of seagrass dynamics, including its seasonal cycle. Thus, the model only operates with the maximum seagrass summer extent and does not consider the decreasing population in autumn and winter, and it does not account for the damage seagrass experiences during storm events that can be quite severe. These are important considerations that limit the validity of our analysis to the vegetation period, while significant storm events often occur in autumn and winter when the seagrass population is already thinned out.

While there remain some important steps for improving the model system to account for more processes and while the lack of representation partially leads to overestimation (attenuation of kinematics) and underestimation (stresses needed for mobilisation), this study is a first step in assessing the effect of seagrass in a fully coupled hydrodynamic, wave, and sediment system.

5 Conclusions and outlook

A multi-physics-coupled model was set up for the German Bight and used to study the effect of vegetation on hydro-, wave-, and sediment dynamics. Using the model, different seagrass expansion scenarios were tested and statistically analysed in terms of the monthly average and 95th percentile. Comparing the scenarios with and without seagrass demonstrated a strong local dissipative effect of seagrass on currents and waves, which increased with seagrass extent and patch density. This resulted in a reduction in bottom stress, leading to significantly lower sediment concentrations. The resulting reduction in bottom stress manifested in strongly decreased bottom sediment concentrations

indicating lower rates of resuspension and the potential to reduce coastal erosion. Wave and current attenuation under storm conditions appeared slightly increased compared to that under calm weather conditions, but this attenuation was reduced in relative terms. As seagrass impacts on sea level are minor, seagrass contributions to flood protections are only indirect. The potential of seagrass to support the vertical height growth of the Wadden Sea to maintain bathymetric control under future increases in sea level is seen as the major long-term contribution of seagrass to coastal protection.

While this study demonstrates the beneficial effects of an extended seagrass coverage for coastal protection in the German Bight, in reality, seagrass is still not recovering in the EFWS area. Out of the several environmental conditions that can negatively impact seagrass (hydrodynamic stress, low-light, eutrophication), eutrophication is widely considered the dominant factor that led to the initial loss of seagrass after the 1950s to the 1970s in the Dutch (Philippart 1994) and German parts of the Wadden Sea (Dolch et al. 2013; van Beusekom et al. 2019). In the southern Wadden Sea, eutrophication and chlorophyll a levels are higher compared to those in the northern Wadden Sea, which van Beusekom et al. (2019) attributed to the greater accumulation of organic matter along the southern coast, and this organic matter originates from that matter produced in the North Sea. In the NFWS, a decline in nitrogen and phosphorus concentrations after their peak in the 1980s and 1990s led to the recovery of seagrass in the late 1990s (Dolch et al. 2013; van Beusekom et al. 2019). This was related to reduced nutrient loads in the Weser and Elbe Rivers. Although nitrogen and phosphorus loads also decreased in the Rhine and Maas Rivers, the reduction seems insufficient to stimulate seagrass growth in the EFWS. Therefore, and due to regulations that forbid direction interventions in the system Wadden Sea (e.g., sediment seeding), efforts to increase water quality and decrease terrestrial and fluvial nutrient input are suggested as the most important step to further improve conditions in the EFWS.

This study is a first step to assess the effect of seagrass in a fully coupled hydrodynamic, wave, and sediment system at a large scale. As a next step, the limitations of the study motivate a reassessment, with further model improvements to reduce overestimations: This encompasses an extension of the model to account for the flexibility of seagrass, an expanded consideration of the biological compartment, and the simulation of seagrass seasonality and its dependence on nutrients. Additionally, the next steps involve exploring extended simulation periods under climate projections and actively simulating related morphological changes in the bathymetry induced by seagrass.

Supplementary Information The online version contains supplementary material available at https://doi.org/10.1007/s10236-023-01577-5.

Acknowledgements We acknowledge the EU Green Deal project REST-COAST: Large scale recovery of coastal ecosystems through rivers to sea connectivity, providing the funding for the research undertaken in this study. Furthermore, we acknowledge the Copernicus marine service evolution project Coastal-risks as additional funding source. We further would like to acknowledge the Landesamt für Landwirtschaft, Umwelt und ländliche Räume Schleswig-Holstein (LLUR) and Landesbetrieb für Küstenschutz, Nationalpark und Meeresschutz Schleswig-Holstein - Nationalparkverwaltung (LKN) for funding seagrass monitoring in Schleswig-Holstein. We thank the editor Jia Wang and the two anonymous reviewers for their comments, which helped to further improve the manuscript. JS gratefully acknowledges the project DOORS (grant no. 101000518)

Funding Open Access funding enabled and organized by Projekt DEAL.

Data Availability All data generated or analysed for this study are available from the corresponding author on reasonable request.

Declarations

Conflict of interest The authors declare that the research was conducted in the absence of any commercial or financial relationships that could be construed as a potential conflict of interest.

References

Abdolali A, Hesser TJ, Anderson Bryant M et al (2022) Wave attenuation by vegetation: model implementation and validation study. Frontiers in Built Environ 8:891612

Adams MP, Hovey RK, Hipsey MR et al (2016) Feedback between sediment and light for seagrass: where is it important? Limnology and Oceanography 61(6):1937–1955. https://doi.org/10.1002/lno.10319

Alfieri L, Burek P, Feyen L et al (2015) Global warming increases the frequency of river floods in Europe. HydrolEarth Syst Sci 19(5):2247–2260. https://doi.org/10.5194/hess-19-2247-2015. https://hess.copernicus.org/articles/19/2247/2015/, publisher: Copernicus GmbH

Allan RP, Hawkins E, Bellouin N, et al (2021) IPCC, 2021: Summary for policymakers. In: Masson-Delmotte V, Zhai P, Pirani A, et al (eds) Climate change 2021: the physical science basis. Contribution of working group I to the 6th Assessment report of the intergovernmental panel on climate change. Cambridge University Press, pp 3–32. https://centaur.reading.ac.uk/101317/

Amos CL, Bergamasco A, Umgiesser G et al (2004) The stability of tidal flats in Venice Lagoon-the results of in-situ measurements

using two benthic, annular flumes. J Marine Syst 51(1):211–241. https://doi.org/10.1016/j.jmarsys.2004.05.013. https://www.sciencedirect.com/science/article/pii/S092479630400185X

Ariathurai R, Arulanandan K (1978) Erosion rates of cohesive soils. J Hydraul Div 104(2):279–283

Arns A, Wahl T, Dangendorf S et al (2015) The impact of sea level rise on storm surge water levels in the northern part of the German Bight. Coastal Eng 96:118–131. https://doi.org/10.1016/j.coastaleng.2014.12.002, https://www.sciencedirect.com/science/article/pii/S0378383914002191

Battjes JA, Janssen JPFM (1978) Energy loss and set-up due to breaking of random waves. Coastal Eng Proc 1(16):32–32. https://doi.org/10.9753/icce.v16.32. https://icce-ojs-tamu.tdl.org/icce/article/view/3294, number: 16

Benninghoff M, Winter C (2019) Recent morphologic evolution of the German Wadden Sea. Sci Rep 9(1):9293. https://doi.org/10.1038/s41598-019-45683-1, https://www.nature.com/articles/s41598-019-45683-1

Bergillos RJ, López-Ruiz A, Principal-Gómez D et al (2018) An integrated methodology to forecast the efficiency of nourishment strategies in eroding deltas. Sci Total Environ 613–614:1175–1184. https://doi.org/10.1016/j.scitotenv.2017.09.197. https://www.sciencedirect.com/science/article/pii/S0048969717325469

Beudin A, Kalra TS, Ganju NK et al (2017) Development of a coupled wave-flow-vegetation interaction model. Comput Geosci 100:76–86. https://doi.org/10.1016/j.cageo.2016.12.010. https://www.sciencedirect.com/science/article/pii/S0098300416308184

van Beusekom JEE, Carstensen J, Dolch T, et al (2019) Wadden sea eutrophication: long-term trends and regional differences. Frontiers in Marine Science 6. https://www.frontiersin.org/articles/10.3389/fmars.2019.00370

Bittner RE, Roesler EL, Barnes MA (2020) Using species distribution models to guide seagrass management. Estuar Coast Mar Sci 240:106790. https://doi.org/10.1016/j.ecss.2020.106790. https://www.sciencedirect.com/science/article/pii/S027277141930825X

de Boer WF (2007) Seagrass-sediment interactions, positive feedbacks and critical thresholds for occurrence: a review. Hydrobiologia 591(1):5–24. https://doi.org/10.1007/s10750-007-0780-9

Boudouresque CF, Blanfuné A, Pergent G et al (2021) Restoration of seagrass meadows in the Mediterranean Sea: a critical review of effectiveness and ethical issues. Water 13(8):1034. https://doi.org/10.3390/w13081034. https://www.mdpi.com/2073-4441/13/8/1034

Bouma TJ, van Belzen J, Balke T et al (2014) Identifying knowledge gaps hampering application of intertidal habitats in coastal protection: opportunities & steps to take. Coastal Eng 87:147–157. https://doi.org/10.1016/j.coastaleng.2013.11.014. https://www.sciencedirect.com/science/article/pii/S037838391300197X

Chefaoui RM, Duarte CM, Serrão EA (2018) Dramatic loss of seagrass habitat under projected climate change in the Mediterranean Sea. Glob Chang Biol 24(10):4919–4928. https://doi.org/10.1111/gcb.14401

Chen WL, Muller P, Grabowski RC, et al (2022) Green nourishment: an innovative nature-based solution for coastal erosion. Frontiers in Marine Science 8. https://www.frontiersin.org/articles/10.3389/fmars.2021.814589

Christianen MJA, Jv Belzen, Herman PMJ et al (2013) Low-canopy seagrass beds still provide important coastal protection services. PLOS ONE 8(5):e62413. https://doi.org/10.1371/journal.pone.0062413. https://journals.plos.org/plosone/article?id=10.1371/journal.pone.0062413, publisher: Public library of science

Costanza R, d'Arge R, de Groot R et al (1997) The value of the world's ecosystem services and natural capital. Nature 387(6630):253–260. https://doi.org/10.1038/387253a0. https://www.nature.com/articles/387253a0, number: 6630 Publisher: Nature publishing group

Couasnon A, Eilander D, Muis S et al (2020) Measuring compound flood potential from river discharge and storm surge extremes at the global scale. Nat Hazards Earth Syst Sci 20(2):489–504. https://doi.org/10.5194/nhess-20-489-2020. https://nhess.copernicus.org/articles/20/489/2020/, publisher: Copernicus GmbH

Dolch T, Buschbaum C, Reise K (2013) Persisting intertidal seagrass beds in the northern Wadden Sea since the 1930s. J Sea Res 82:134–141. https://doi.org/10.1016/j.seares.2012.04.007. https://www.sciencedirect.com/science/article/pii/S1385110112000536

Dolch T, Folmer EO, Frederiksen MS, et al (2017) Seagrass. In: et al KS (ed) Wadden Sea quality status report. Common wadden sea secretariat, Wilhelmshaven, Germany. qsr.waddensea-worldheritage.org/reports/seagrass, last updated 21.12.2017. Downloaded 01.01.2023

Duarte CM, Kennedy H, Marbá N et al (2013) Assessing the capacity of seagrass meadows for carbon burial: current limitations and future strategies. Ocean Coast Manag 83:32–38. https://doi.org/10.1016/j.ocecoaman.2011.09.001. https://www.sciencedirect.com/science/article/pii/S0964569111001323

Ferrario F, Beck MW, Storlazzi CD et al (2014) The effectiveness of coral reefs for coastal hazard risk reduction and adaptation. Nature Commun 5(1):3794. https://doi.org/10.1038/ncomms4794, https://www.nature.com/articles/ncomms4794%22 Publisher: Nature publishing group

Fonseca MS, Fisher JS, Zieman JC, et al (1982) Influence of the seagrass, Zostera marina L, on current flow. Estuar Coast Shelf Sci 15(4):351–364. https://doi.org/10.1016/0272-7714(82)90046-4. https://www.sciencedirect.com/science/article/pii/0272771482900464

French PW (2002) Coastal defences: processes. Routledge, London, Problems and Solutions. https://doi.org/10.4324/9780203187630

Gacia E, Granata TC, Duarte CM (1999) An approach to measurement of particle flux and sediment retention within seagrass (Posidonia oceanica) meadows. Aquat Bot 65(1):255–268. https://doi.org/10.1016/S0304-3770(99)00044-3

Gagnon K, Christie H, Didderen K et al (2021) Incorporating facilitative interactions into small-scale eelgrass restoration-challenges and opportunities. Restor Ecol 29(5):e13398. https://doi.org/10.1111/rec.13398

Govers LL, Heusinkveld JH, Gräfnings ML et al (2022) Adaptive intertidal seed-based seagrass restoration in the Dutch Wadden Sea. Plos one 17(2):e0262845

Hansen JCR, Reidenbach MA (2012) Wave and tidally driven flows in eelgrass beds and their effect on sediment suspension. Mar Ecol Prog Ser 448:271–287. https://doi.org/10.3354/meps09225

Hansen JCR, Reidenbach MA (2013) Seasonal growth and senescence of a Zostera marina seagrass meadow alters wave-dominated flow and sediment suspension within a coastal bay. Estuar and Coasts 36(6):1099–1114. https://doi.org/10.1007/s12237-013-9620-5

Hasselmann K, Barnett TP, Bouws E, et al (1973) Measurements of wind-wave growth and swell decay during the joint North Sea wave project (JONSWAP). Ergänzungsheft zur Deutschen Hydrographischen Zeitschrift, Reihe A Nr. 12. https://pure.mpg.de/pubman/faces/ViewItemOverviewPage.jsp?itemId=item_3262854

Horstman EM, Dohmen-Janssen CM, Narra PMF et al (2014) Wave attenuation in mangroves: a quantitative approach to field observations. Coastal Eng 94:47–62. https://doi.org/10.1016/j.coastaleng.2014.08.005

Irving AD, Tanner JE, Collings GJ (2014) Rehabilitating seagrass by facilitating recruitment: improving chances for success. Restor Ecol 22(2):134–141. https://doi.org/10.1111/rec.12036

Izaguirre C, Méndez FJ, Menéndez M, et al (2011) Global extreme wave height variability based on satellite data. Geophysical Research Letters 38(10). https://doi.org/10.1029/2011GL047302

Jacob B, Stanev EV (2021) Understanding the impact of bathymetric changes in the German Bight on coastal hydrodynamics: one step toward realistic morphodynamic modeling. Frontiers in Marine Science 8. https://www.frontiersin.org/articles/10.3389/fmars.2021.640214

Koch EW (2001) Beyond light: physical, geological, and geochemical parameters as possible submersed aquatic vegetation habitat requirements. Estuaries 24(1):1–17. https://doi.org/10.2307/1352808

Krämer L (2018) The EU Directive 2014/89 establishing a framework for maritime spatial planning. J Eur Environ Planning Law 15(1):24–41. https://doi.org/10.1163/18760104-01501003. https://brill.com/view/journals/jeep/15/1/article-p24_24.xml, publisher: Brill Nijhoff

Lawson SE, McGlathery KJ, Wiberg PL (2012) Enhancement of sediment suspension and nutrient flux by benthic macrophytes at low biomass. Marine Ecol Prog Ser 448:259–270. https://doi.org/10.3354/meps09579,https://www.int-res.com/abstracts/meps/v448/p259-270/

Leonardi N, Carnacina I, Donatelli C et al (2018) Dynamic interactions between coastal storms and salt marshes: a review. Geomorphology 301:92–107. https://doi.org/10.1016/j.geomorph.2017.11.001

Menéndez M, Woodworth PL (2010) Changes in extreme high water levels based on a quasi-global tide-gauge data set. Journal of Geophysical Research: Oceans 115(C10). https://doi.org/10.1029/2009JC005997

Milbradt P, Valerius J, Zeiler M (2015) Das funktionale bodenmodell: Aufbereitung einer konsistenten datenbasis für die Morphologie und Sedimentologie. Die Küste 83(1):19–38

Montgomery JM, Bryan KR, Mullarney JC et al (2019) Attenuation of storm surges by coastal mangroves. Geophys Res Lett 46(5):2680–2689. https://doi.org/10.1029/2018GL081636

Morris RL, Konlechner TM, Ghisalberti M et al (2018) From grey to green: efficacy of eco-engineering solutions for nature-based coastal defence. Glob Change Biol 24(5):1827–1842. https://doi.org/10.1111/gcb.14063

Narayan S, Beck MW, Reguero BG et al (2016) The effectiveness, costs and coastal protection benefits of natural and nature-based defences. PLOS ONE 11(5):e0154735. https://doi.org/10.1371/journal.pone.0154735. https://journals.plos.org/plosone/article?id=10.1371/journal.pone.0154735, publisher: Public library of science

Nepf HM, Vivoni ER (2000) Flow structure in depth-limited, vegetated flow. J Geophys Res: Oceans 105(C12):28547–28557. https://doi.org/10.1029/2000JC900145

Nicholls RJ (2011) Planning for the impacts of sea level rise. Oceanography 24(2):144–157

Paul M, Bouma TJ, Amos CL (2012) Wave attenuation by submerged vegetation:- combining the effect of organism traits and tidal current. Marine Ecol Prog Ser 444:31–41. https://doi.org/10.3354/meps09489. https://www.int-res.com/abstracts/meps/v444/p31-41/

Philippart CJ (1994) Eutrophication as a possible cause of decline in the seagrass Zostera noltii of the Dutch Wadden Sea. Wageningen University and Research

Pickering MD, Wells NC, Horsburgh KJ et al (2012) The impact of future sea-level rise on the European Shelf tides. Cont Shelf Res 35:1–15. https://doi.org/10.1016/j.csr.2011.11.011. https://www.sciencedirect.com/science/article/pii/S0278434311003578

Pillai UPA, Pinardi N, Alessandri J et al (2022) A digital twin modelling framework for the assessment of seagrass nature based solutions against storm surges. Scie Total Environ 847:157603. https://doi.org/10.1016/j.scitotenv.2022.157603. https://www.sciencedirect.com/science/article/pii/S0048969722047015

Pinto L, Fortunato AB, Zhang Y et al (2012) Development and validation of a three-dimensional morphodynamic modelling system for non-cohesive sediments. Ocean Model 57–58:1–14. https://doi.org/10.1016/j.ocemod.2012.08.005. https://www.sciencedirect.com/science/article/pii/S1463500312001175

Roland A, Zhang YJ, Wang HV, et al (2012) A fully coupled 3D wave-current interaction model on unstructured grids. Journal of Geophysical Research: Oceans 117(C11). https://doi.org/10.1029/2012JC007952

Schloen J, Stanev EV, Grashorn S (2017) Wave-current interactions in the southern North Sea: the impact on salinity. Ocean Model 111:19–37. https://doi.org/10.1016/j.ocemod.2017.01.003. https://www.sciencedirect.com/science/article/pii/S1463500317300094

Soulsby R (1997) Dynamics of marine sands: a manual for practical applications. Oceanogr Lit Rev 9(44):947

Soulsby R, Whitehouse R (1997) Threshold of sediment motion in coastal environments. In: Pacific coasts and ports' 97: proceedings of the 13th Australasian coastal and ocean engineering conference and the 6th Australasian port and harbour conference; vol 1, Centre for advanced engineering, University of Canterbury Christchurch, NZ, pp 145–150

Stanev EV, Wolff JO, Brink-Spalink G (2006) On the sensitivity of the sedimentary system in the East Frisian Wadden Sea to sea-level rise and wave-induced bed shear stress. Ocean Dyn 56(3):266–283. https://doi.org/10.1007/s10236-006-0061-6

Stanev EV, Jacob B, Pein J (2019) German Bight estuaries: an inter-comparison on the basis of numerical modeling. Continental Shelf Research 174:48–65. https://doi.org/10.1016/j.csr.2019.01.001. https://www.sciencedirect.com/science/article/pii/S0278434318302772

Staneva J, Behrens A, Groll N (2014) Recent advances in wave modelling for the North Sea and German Bight. Die Küste, 81 Modelling p 23

Suzuki T, Zijlema M, Burger B et al (2012) Wave dissipation by vegetation with layer schematization in swan. Coastal Eng 59(1):64-71

Tanino Y, Nepf HM (2008) Laboratory investigation of mean drag in a random array of rigid, emergent cylinders. J Hydraul Eng 134(1):34–41. https://doi.org/10.1061/(ASCE)0733-9429(2008)134:1(34), publisher: American society of civil engineers

Temmerman S, Bouma TJ, Govers G, et al (2005) Impact of vegetation on flow routing and sedimentation patterns: three-dimensional modeling for a tidal marsh. Journal of Geophysical Research: Earth Surface 110(F4). https://doi.org/10.1029/2005JF000301

Temmerman S, Meire P, Bouma TJ et al (2013) Ecosystem-based coastal defence in the face of global change. Nature 504(7478):79–83. https://doi.org/10.1038/nature12859. https://www.nature.com/articles/nature12859, number: 7478 Publisher: Nature publishing group

Temmerman S, Horstman EM, Krauss KW, et al (2023) Marshes and mangroves as nature-based coastal storm buffers. Ann Rev Mar Sci 15(1):null. https://doi.org/10.1146/annurev-marine-040422-092951

Umlauf L, Burchard H (2003) A generic length-scale equation for geophysical turbulence models. Journal of Marine Research 61(2):235–265. https://doi.org/10.1357/002224003322005087

Valerius J, Kösters F, Zeiler M (2015) Erfassung von Sandverteilungsmustern zur groSSräumigen Analyse der Sedimentdynamik auf dem Schelf der Deutschen Bucht. Die Küste 83(1):39–63

Vargas-Luna A, Crosato A, Calvani G et al (2016) Representing plants as rigid cylinders in experiments and models. Adv Water Res 93:205–222

Vousdoukas MI, Mentaschi L, Voukouvalas E et al (2017) Extreme sea levels on the rise along Europe's coasts. Earth's Future 5(3):304–323. https://doi.org/10.1002/2016EF000505

Wachler B, Seiffert R, Rasquin C et al (2020) Tidal response to sea level rise and bathymetric changes in the German Wadden Sea. Ocean Dyn 70(8):1033–1052. https://doi.org/10.1007/s10236-020-01383-3

Warner JC, Sherwood CR, Signell RP et al (2008) Development of a three-dimensional, regional, coupled wave, current, and sediment-transport model. Comput Geosci 34(10):1284–1306. https://doi.org/10.1016/j.cageo.2008.02.012. https://www.sciencedirect.com/science/article/pii/S0098300408000563

van Wesenbeeck BK, van der Meulen MD, Pesch C, et al (2016)Nature-based approaches in coastal flood risk management: physical restrictions and engineering challenges. In: Renaud FG, Sudmeier-Rieux K, Estrella M, et al (eds) Ecosystem-based disaster risk reduction and adaptation in practice. Advances in natural and technological hazards research, Springer International Publishing, Cham, p 181–198. https://doi.org/10.1007/978-3-319-43633-3_8

Zhang Y, Baptista AM (2008) SELFE: a semi-implicit Eulerian-Lagrangian finite-element model for cross-scale ocean circulation. Ocean Model 21(3–4):71–96. https://doi.org/10.1016/j.ocemod.2007.11.005. https://ohsu.pure.elsevier.com/en/publications/selfe-a-semi-implicit-eulerian-lagrangian-finite-element-model-fo-2

Zhang Y, Ye F, Stanev E et al (2016) Seamless cross-scale modelling with SCHISM. Ocean Modelling 102. https://doi.org/10.1016/j.ocemod.2016.05.002

Zhang YJ, Gerdts N, Ateljevich E et al (2020) Simulating vegetation effects on flows in 3D using an unstructured grid model: model development and validation. Ocean Dyn 70(2):213–230. https://doi.org/10.1007/s10236-019-01333-8